Project	H2020 - SURE (Grant-Number 654662)
Deliverable	D7.2 - Report on Laterals Stability Modelling
Work package	WP7 - Integration
Lead author	John-Paul Latham
Contributor(s)	Ado Farsi, Jiansheng Xiang, Bin Chen
Dissemination level	PU (public)
Type	R (document, report)
Due date	2019-02-28
Actual submission date	2019-05-02
Resubmission date(s)	
Change History	

Licence information	Report D7.2 of the Consortium of the H2020 SURE Project This publication is licensed under a Creative Commons License, International Attribution 4.0: CC BY
DOI (Repository)	10.2312/GFZ.4.8.2019.009
Recommended Citation	Latham, J.-P., Farsi, A., Xiang, J., Chen, B; The Horizon 2020 Project SURE: Deliverable 7.2 - Report on Laterals Stability Modelling, 2019, Potsdam: GFZ German Research Centre for Geosciences, DOI: https://doi.org/10.2312/GFZ.4.8.2019.009
Access to associated data	

The SURE project has received funding from the European Union's Horizon 2020 research and innovation programme under grant agreement No 654662.

Table of Contents

The SURE project has received funding from the European Union's Horizon 2020 research and innovation programme under grant agreement No 654662.

1 Executive Summary

In this deliverable, the objectives of the Imperial College team are to consider jetted boreholes in the context of conventional borehole wall-rock stability analysis and to utilise an in-house advanced combined finite-discrete element code to examine the wall-rock failure process for jetted holes. The geomechanical modelling of Lateral Stability in D7.2 presented here is in addition to the main focus on modelling the water-jetting breakdown of the rock itself, reported in D7.1.

The vulnerability of a horizontal borehole to breakouts or collapse instability depends on the in-situ stress state, fluid pressure, the hole's direction with respect to the principal stress directions and the strength properties of the intact wall-rock including its anisotropy. In the first part of this work (Section 3), a set of semi-empirical equations governing the wall-damage states of radial jet drilled (RJD) laterals is assembled for reservoir engineers, especially those wishing to exploit RJD drilling methods for geothermal reservoirs. The states of wall-rock can be considered as: Stable (S), Stable with Break-outs (SB), Unstable with collapse (U). The criterion for the threshold between S and SB is when the shear failure breakout condition is met. Between SB and U, a conservative criterion is set to be when the breakout angle exceeds 90 degrees. The equations and resulting guidance charts focus on behaviour at a given depth and take into account in-situ stress ratio and the intrinsic intact strength of the rock fabric, as characterised by the unconfined compressive strength σ_c. First, in-situ stress ratios in different tectonic regimes and crustal scenarios are presented to introduce the range of parameters to consider. Consequences of the Kirsch equations for borehole wall stresses around a circular opening are then applied. Finally, for different tectonic faulting regimes and horizontal jet-hole directions, wall-rock damage states are predicted as a function of depth, representative ratio of horizontal to vertical stress in the planes perpendicular to the axes of horizontally jetted holes together with σ_c. Any enlargement of the hole's cross-section by break-out phenomena (or back-thruster erosion) would be advantageous for enhancing heat exchange provided the borehole wall integrity is not lost completely leading to jet-hole collapse. The important interval of conditions between breakouts starting and probable jet-hole collapse is investigated and found to be not always intuitive.

The second part of this work (Section 4) aims to use numerical modelling to explore the stability of horizontal jetted holes for in-situ conditions in more detail. In true triaxial jetting tests performed for WP4 and WP5, when large far field stress ratios of 3 and 7 (30:10, 35:5 MPa) were applied perpendicular to the jetting direction, pronounced breakout features were developed in the jet-holes. For these particular applied stresses and for this Bentheim sandstone the laboratory jetted holes develop significant breakouts while the integrity of the rock block and the remaining borehole wall rock remained stable. The questions of interest are then: what is the uncertainty in the serviceability of the hole and how close is the

The SURE project has received funding from the European Union's Horizon 2020 research and innovation programme under grant agreement No 654662.

DOI: 10.2312/GFZ.4.8.2019.009

combination of test conditions to that causing a complete 360-degree wall collapse, probably leading to fragment infill and fluid flow blockage? The laboratory experiments are introduced in Section 4.2. To consider the progressive fracture growth process once conditions are met for breakout initiation and under increasing stress levels to enlarge the breakout areas, we employ *Solidity*, an in-house combined finite-discrete element method (FDEM or FEMDEM) code. Solidity handles multi-body interactions which makes it well-suited for jointed rock, together with the transient dynamic brittle-elastic response of rock whereby each new fracture is explicitly represented together with shear displacements on them. Initiation without a need to seed flaws, propagation and interaction of fractures and fragmentation are included. This allows numerical model study of the effect of a loading history. In this work we apply an initial stress of zero with a fixed stress ratio that has boundary stress magnitudes linearly ramped up until they exceed those required to initiate local brittle failure. For a large rock block specimen with a small hole, the simple theory in Section 3 predicts that after a stable elastic deformation, first an initiation of breakouts (S→SB) will occur, then stable holes continue to accommodate progressive breakout deepening and widening through to final total wall collapse (SB→U). This evolution of brittle deformation processes was neglected in Section 3 and is a key focus of FDEM modelling in Section 4.

In addition to these 2D jet-wall fracture models, to gain more understanding of the 3D stress field effects, a 3D finite element analysis is also performed using a solver in MATLAB. Finite element methods are used to solve the 3D stress field surrounding cylindrical and X-Ray CT scanned irregular shaped and broken out jet-hole geometries. A jet-hole's wall rock fracture susceptibility is explored by plotting the local stress as a percentage of failure stress for both shear failure and tensile failure at different element locations around jet-holes. Several in-situ stress states are illustrated. The main objectives of the modelling research in Section 4 are to:

- Develop a method to compute local stresses around cylindrical jetted and irregular shaped boreholes for generic far-field stress conditions and as guided by the true triaxial laboratory experiments in Delft (WP4, WP5). (See Section 4.2.1)
- Develop a new protocol for accelerating the run-time of FDEM while removing the effect of unrealistic stress waves caused by sudden loading. (See Section 4.2.4)
- Perform 2D FDEM simulation to match laboratory conditions and laboratory test data from WP4 and WP5 to investigate mechanism of breakout progression and ultimate collapse. (See Sections 4.5.2, 4.5.3)
- Perform 2D FDEM on typical cross-hole geometries obtained in triaxial jetting tests and complex e.g. star-like cross-sections. (See Section 4.5.4)
- Perform 3D polyaxial stress state stability assessment of variable geometry laterals. (See Section 4.4.2)

The conclusions from the modelling research were:

The SURE project has received funding from the European Union's Horizon 2020 research and innovation programme under grant agreement No 654662.

- The modelling study demonstrated that a 3D elastic FEM analysis is an important tool for understanding wall rock states of stress and proximity to conditions of tensile or shear failure. A new non-commercial FEM tool was developed in MATLAB for this purpose.
- The new coupled protocol tool for implicit FEM – explicit FDEM enables the FDEM simulation with ramping of loads to be executed much faster than a pure FDEM simulation.
- FDEM simulation highlights the simple theory's lack of consideration of progressive deformation and stress redistribution effects.
- Collapse state prediction of the simple theory may be too simplistic. The safe window between initiation of breakouts and collapse suggested by the simple theory may be quite false.
- FDEM suggests collapse follows soon after breakout development, but there are many reasons why this suggestion needs further confirmation.
- FDEM results were especially interesting in showing a previously undocumented mode of progressive breakouts based on alternating shear fracturing with tensile wing crack loosening and the formation of discrete fragments that are seen to move into the hole.
- The jetting in true-triaxial states and simulation by FDEM concentrated on a weak porous sandstone with a non-linear shear failure envelope which may be an especially difficult rock type to simulate well with a homogeneous brittle elastic formulation. Results are likely to be more reliable for stronger more brittle rocks.
- More reliable FDEM work on breakout/stability/collapse for a given far field stress may require the development of a more realistically phased loading history that reflects an excavation process of an unloading from an in-situ stress equilibrium state.

2 Background to Lateral Stability and Numerical Modelling

Jet drilling nozzle geometry and related technologies are undergoing innovative design modifications in search of a means to jet into deeper and harder rock. Currently, initiation and penetration of the jet at viable speeds remains a challenge for harder rocks and in down hole field conditions e.g. from 500 – 5000 m depth. Meanwhile, common RJD practice in sedimentary O&G reservoirs employs static and rotating nozzles which have forward and backward facing orifices to create both rock fabric damage in front and a means of propulsion behind the advancing head (Fig. 1). The prediction of field performance of jetting and the resulting hole geometries has been largely derived from laboratory tests on unconfined rock. Such geometries vary from back-thruster wash-out dominated star-shapes in soft limestones, conical profiles indicative of stop-start progression, to quite smooth cylindrical forms, depending on types of nozzle and rock type resistance. Actual geometries and stabilities of jet-drilled laterals in-situ and at depth in reservoirs may well be different from these unconfined tests. Both simple theory (Section 3) and numerical modelling (Section 4) are used to investigate lateral stability in this work.

The SURE project has received funding from the European Union's Horizon 2020 research and innovation programme under grant agreement No 654662.

For RJD operations, once the lateral has been jetted, the possible losses of fluid flow performance over time are considered to be mainly due to a combination of: (i) fines migration clogging, more common in reservoirs with argillite rock types and a cited problem in Klaipeda, (Brehme et al., 2018) (ii) creep, (especially thermally assisted creep leading to aperture reduction over time. This was considered in the context of poro-elastoplastic and thermo-elastoplastic 2D modelling of RJD deformation in chalk rock by Medetbekova et al., 2017), (iii) geochemical precipitation (scale) causing aperture reduction (discussed in Blöcher et al., 2016) and (iv) structural effects due to brittle wall damage, breakouts, fragmentation, and consequent possible blockages and clogging. The latter wall rock breakage, according to 3D FEM analysis considering circular tunnel advance, develops to its maximum at around two diameters behind the advancing hole for stress fields considered by Eberhard (2001). At this distance and further behind the advancing front, wall differential stresses are fully amplified to their 2D plane strain state. Increased intensity of breakout features such as depth and breakout arc angle (discussed later) will occur the higher are the ratios of maximum wall rock tangential stress to unconfined compressive stress, UCS.

While considerable effort in the SURE project addresses 'jettability' and the factors governing rates of jet penetration under field conditions of in-situ stress and pore pressure, this report focuses on the stability of the lateral in terms of the ultimate strength of the wall rock. Rather than considering time-dependent processes affecting long-term stability, it examines how rock deformation accommodates the changes in the triaxial stress state occurring near the time of the RJD excavation process, through brittle failure and progressive fracturing.

Figure 1. RJD holes and nozzles: Left to right: principal of forward and backward thrusters in static nozzle; star-shaped profiles in soft limestone with unconfined rock and static nozzle; conical stop-start geometries formed at head of rotating nozzle; detail of Beetle, BT 18 mm rotating nozzle available from "StoneAge" used in true-triaxial laboratory tests performed at TUDelft by Richard Bakker (TUDelft) and Simon Hahn (GZB) in WP4 and WP5.

Many reservoir depths and in-situ stress conditions envisaged for RJD geothermal energy exploitation including future EGS and HDR may exceed failure conditions under which 'breakout' wall failure processes and possible collapse is predicted to occur. To generate the simplest guidelines as a prelude to considering modelling results that include more detailed mechanics, in the first part of the report the initial jet-excavated hole geometry is assumed to be cylindrical and a plane strain analysis is applied. As RJD laterals cannot be controlled by

The SURE project has received funding from the European Union's Horizon 2020 research and innovation programme under grant agreement No 654662.

raised internal fluid pressure e.g. through mud or water pressures within the jet-hole, borehole breakout criteria based on effective stresses is quite simple to apply. These criteria for strength to resist the wall-rock's tangential stress given by the Kirsch solution are based on simple strength of materials theory.

Scale effects for the diameter of holes in intact rock, where smaller holes are stronger have been reported for holes of < 20 mm, as microstructure has an impact at this scale, (Dresen et al., 2010). In general and for rocks of typical grain sizes, stress around a hole resulting from far field stresses is a scale independent problem such that circular tunnels and boreholes can be treated identically in a continuum model if it is assumed there are no discontinuities in the tunnel (and borehole). Hence much of the literature on tunneling stability has particular relevance to (horizontal) borehole stability. The simulations presented in this research are designed to model stability of wall-rock found in actual jetting experiments of ~20-30 mm diameter jetted holes with stresses representing far field in-situ stresses applied to the boundaries of cubical rock blocks of 300 mm.

The first part of this report (Section 3) develops an introductory predictive guide to stability through (i) an introduction to states of in-situ stress, (ii) application of Kirsch solutions to breakouts and collapse prediction in horizontal holes and (iii) predicted wall-damage states for RJD laterals at various depths. For the second part (Section 4), jetted holes from true triaxial stress experiments (WP4, WP5) are introduced and numerical modelling is applied.

3 Guidance on predicted wall-rock stability of Lateral

3.1 In-Situ Stress and Faulting Regimes

Relative stress magnitudes for Anderson's faulting regimes (Fig. 2) can be summarised as shown in Table 1.

Table 1 Relative stress magnitudes and faulting regimes, where $S_1>S_2>S_3$

Regime	**Stress**		
	S_1	S_2	S_3
Normal (NF)	S_v	S_{Hmax}	S_{hmin}
Strike-Slip (SS)	S_{Hmax}	S_v	S_{hmin}
Reverse (RF)	S_{Hmax}	S_{hmin}	S_v

It is neither straightforward nor inexpensive to obtain accurate in-situ stress measurement magnitudes and directions for a given rock engineering project or reservoir site, although their values are critical for rigorous subsurface design. Therefore, considerable research has been devoted to in-situ stress measurement, (Zoback et al., 1985; Barton et al., 1988; Haimson and Cornet 2003), stress ratio data and the World Stress Map Database (Rummel et al 1986, Zang and Stephansson, 2009; Zang et al., 2012), and prediction models (Zoback et al., 2003, Zoback 2007, Taherynia et al, 2016). As discussed in Zoback (2007, Chapters 4 and 10), the

The SURE project has received funding from the European Union's Horizon 2020 research and innovation programme under grant agreement No 654662.

scatter of stress measurement ratio observations is consistent with bounds set by the critically stressed crust hypothesis. This gives an upper bound for S_H/S_v of 3.1 for in-situ fluid pressure P_0=0 and a lower bound for S_h/S_v of 0.32 for P_0=0. Typically the open hole borehole pressure can be assumed to be given by $\lambda = 0.4$ where $\lambda = P_0/\sigma_v$, i.e. the hydrostatic stress gradient.

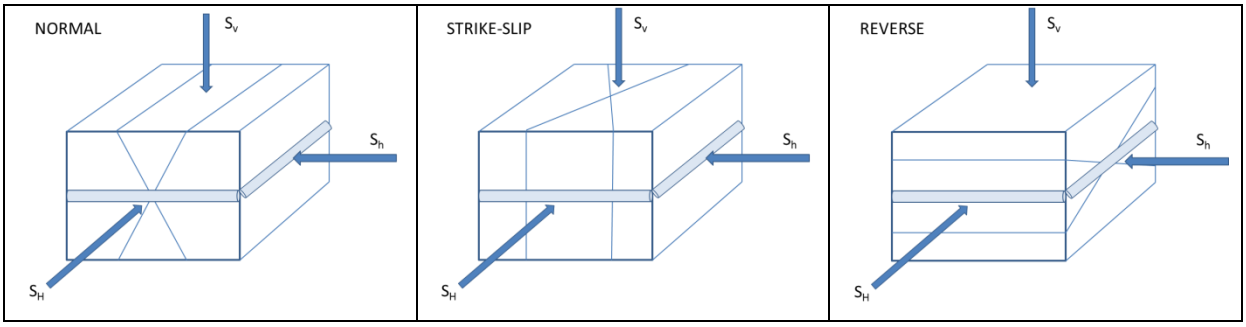

Figure 2. Anderson's Faulting regimes illustrated with two special cases of horizontal RJD jet-hole axes, either parallel to S_H or parallel to S_h

In the quality controlled Quantitative World Stress Map (Q-WSM) resource discussed in Zang et al., (2012), stress magnitude data from 296 global determinations were compiled into two tables with best-fit average stress ratios S_h/S_H, S_h/S_v, and S_H/S_v grouped by rock type (crystalline or sedimentary) and by tectonic faulting regime. Note that in this data-base, data at greater depths is under-represented and limited to several deep e.g. geothermal reservoir and research borehole studies.

Table 2 Tectonic stress ratios from Q-WSM database (Zang et al., 2012) linear regression best-fit

Stress ratio	**NF**	**SS**	**RF**
S_h/S_H	0.64	0.53	0.57
$k_h = S_h/S_V$	0.57	0.71	1.30
$k_H = S_H/S_V$	0.87	1.31	2.23

Table 2 provides the basis of an initial empirical guide to biaxial stress ratios in planes perpendicular to horizontal borehole axes that are likely to be encountered in different faulting regimes. However, these ratios are known to vary non-linearly with depth and therefore a range of k_h and k_H values varying around the best fit values may also be worth considering, as discussed later. The range of data that considers trends with depth (e.g. Rummel et al., 1986) suggests that plausible applicable values of interest for the depths of 0.5 - 1 km should include k_H and k_h values from 0.5 to 2.2 and from depths of 1 km to 5 km, from 0.5 to 1.5.

Where the intermediate principal stress is vertical, i.e. the strike-slip regime, this regime is unlikely to be associated with a far-field biaxial stress ratio across a horizontal jetted hole of greater than 2. Where the maximum principal stress is vertical, i.e. the normal faulting regime, this regime is unlikely to be associated with a far-field biaxial stress ratio across a horizontal jetted hole of greater than 2. Where the minimum principal stress is vertical, i.e. the reverse fault regime, this regime can generate higher far-field biaxial stress ratios across a

The SURE project has received funding from the European Union's Horizon 2020 research and innovation programme under grant agreement No 654662.

horizontal jetted hole but not greater than $k_H = S_H/S_V \sim 3.1$. For depths exceeding 1 km this ratio would be less than 3.1, the average reported for depths from all available data being 2.23 for the reverse faulting regime.

3.2 Kirsch solution for breakouts and collapse

Methods to determine stability of circular tunnel sections, (e.g. Martin et al., 1998) methods to plan well drilling with mud weight control of borehole breakouts (Zoback 2007) and methods to measure in-situ stress using 'breakouts' and tensile hydro-fractures (see e.g. recent work by Kim et al., 2017) all apply simple criteria for the threshold of failure around circular openings based on the Kirsch solution for tangential stresses around the wall of a circular opening, see Fig. 3.

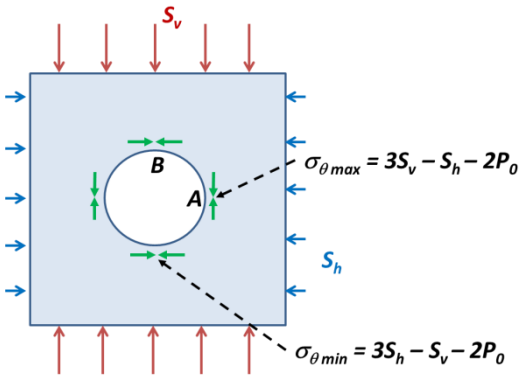

Figure 3. Kirsch solution for tangential stresses around the wall of a horizontal borehole, illustrated here for the Normal Faulting regime with borehole axis parallel to S_H and perpendicular to S_h.

Consider a vertical borehole with far field maximum principal stress (S_{Hmax}) and far field minimum principal stress (S_{hmin}) acting across the hole, and no difference between the formation pore pressure and the borehole fluid pressure, the maximum effective tangential compressive stress generated in the wall of a cylindrical hole, $\sigma_{\theta max}$ is given by

$$\sigma_{\theta max} = 3S_{Hmax} - S_{hmin} - 2P_0 \qquad (1)$$

For the horizontal borehole case illustrated in Fig. 3, this occurs at location A. The minimum effective tangential compressive stress, $\sigma_{\theta min}$ is given by

$$\sigma_{\theta min} = 3S_{hmin} - S_{Hmax} - 2P_0 \qquad (2)$$

For the horizontal borehole case illustrated in Fig. 3, this occurs at location B. The wall rock is in an entirely stable state for conditions where $\sigma_{\theta max} \leq \sigma_c$, i.e. the tangential (hoop) stress does not exceed the rock's unconfined compressive strength, σ_c (interchangeably written as UCS in this work). The equivalent equation can be derived for horizontal boreholes yielding a

The SURE project has received funding from the European Union's Horizon 2020 research and innovation programme under grant agreement No 654662.

first criterion - for stress states at the transition from stable (S) to stable with breakouts (SB). i.e.

$$\sigma_{\theta max} \leq \sigma_c \qquad (3)$$

To provide a *second criterion* – for stress states at the transition from Stable with Breakouts (SB) to Unstable with likely collapse (U), it is possible to consider the range of breakout angles through which the stress state exceeds the unconfined compressive strength. The tangential effective stress σ_θ varies around the circumference (e.g. Barton et al., 1988) according to

$$\sigma_\theta = (\sigma_{Hmax} + \sigma_{hmin}) - 2(\sigma_{Hmax} - \sigma_{hmin}) \cos 2\alpha - \Delta P_w \qquad (4)$$

where σ_{Hmax} and σ_{hmin} are the maximum and minimum effective horizontal principal stresses and α is the angle measured from the S_{Hmax} direction. Here, ΔP_w is the absolute magnitude of the difference between the formation pore pressure and borehole fluid pressure. For the discussion here of an open walled lateral connected to a producer or injector well it is reasonable to assume ΔP_w to be zero and that the borehole fluid pressure during production is that given by the hydraulic gradient, i.e. $\lambda = 0.4$. After the initial failure of the borehole wall upon breakout fracturing the circumferential stress decreases. This process will tend to prevent widening of the breakout although progressive deepening may occur. Setting $\sigma_\theta \geq \sigma_c$ in Eq (4) allows the breakout arc angle θ within which the tangential stress exceeds σ_c to be predicted from theory.

$$\frac{1-(\sigma_{Hmax} + \sigma_{hmin})/\sigma_c}{2(\sigma_{Hmax} - \sigma_{hmin})/\sigma_c} = \cos\theta \qquad (5)$$

When θ exceeds 90° more than half the hole's circumference is represented by a stress state suggesting it will have failed by breakout shearing. The remaining intact arch support may be inadequate to support the applied forces and this could lead to failure all the way around the hole with its enlargement in all directions. The stress concentration around a circular hole does not change with increasing hole size if the discontinuous structure of rock is ignored, so there is the possibility of substantial collapse. Maintaining initial breakout width to <90° has been suggested as an effective criterion for achieving a desired degree of wellbore stability (Zoback 2007).

In Eq (5), θ exceeds 90° when

$$\sigma_{Hmax} + \sigma_{hmin} > \sigma_c \qquad (6)$$

Or in terms of total stresses, when

$$S_{Hmax} + S_{hmin} - 2P_0 > \sigma_c \qquad (7)$$

The SURE project has received funding from the European Union's Horizon 2020 research and innovation programme under grant agreement No 654662.

Note that here we apply the often chosen simplifying assumption that for strong brittle rocks, Biot's effective stress coefficient (alpha), in drained conditions is equal to 1. For relatively weak rock like the Gildehaus Bentheim sandstone which was the subject of the true-triaxial study in WP4 and WP5, this value should also be taken to be ≈1 since here we are considering Biot's effective stress coefficient 'alpha' for shear failure calculation and not for elastic compaction (Baud et al., 2015).

This *second criterion* emphasises the role of mean stress in the horizontal plane for this vertical borehole case. The same criterion is hereby proposed for the threshold between SB and U and is now configured for maximum and minimum stress across horizontal boreholes.
To recap, for breakouts and for collapse conditions, i.e. the *first criterion* and *second criterion* above; the rock has been assumed isotropic elastic with isotropic strength properties. Brittle failure is assumed to be by shear when the maximum tangential stress exceeds the unconfined compressive strength σ_c. This is consistent with a Mohr-Coulomb shear failure criterion for conditions at the wall-rock surface, where the minimum effective principal stress is by definition equal to zero. In this case σ_c can be related to the Mohr-Coulomb shear failure parameters for confined conditions; cohesive strength C_o and angle of internal friction ϕ, where $\mu = \tan^{-1}\phi$, using the relation

$$\sigma_c = 2C_0.\left(\frac{1+sin\emptyset}{1-sin\emptyset}\right)^{0.5} \quad (8)$$

Or $$\sigma_c = 2C_0.\,[(\mu^2+1)^{0.5} + \mu] \quad (9)$$

For a fuller analysis of predicted breakout zone depth, including progression of the fracture softened wall-rock and consequence of spiralling and unstable collapse progression processes, the stress state further into the rock from the wall-rock surface must be considered. Furthermore, a three-dimensional theory of deformation and failure considering confined rock as well as unconfined wall stress states is necessary. A further consideration is that many sedimentary rocks are layered and foliated with anisotropic elasticity and strength properties that affect breakout and collapse susceptibility. The Leknitskii-Amadei solution which applies a plane strain solution to anisotropic elasticity around a circular opening has been considered for breakouts in transversely anisotropic rocks by Setiawan and Zimmerman (2018). They also considered an analytical solution for shear failure initiated according to the Mogi-Coulomb criterion for intact rock failure in 3D, with the Jaeger plane of weakness concept also implemented. This approach allows for all three principal stresses to be accounted for in predicting the onset of shear failure. They conclude that the elastic anisotropy can amplify the stress concentrations that cause breakouts by 25% for anisotropy values that might be expected for rocks of practical interest. Also, that boreholes aligned sub-parallel to faults, joints and bedding planes are more unstable, but their influence is negligible with boreholes subnormal to weakness planes, as would be expected from kinematic stability theory and as seen in practical tunnel engineering.

The SURE project has received funding from the European Union's Horizon 2020 research and innovation programme under grant agreement No 654662.

3.3 RJD Stability Prediction - Discussion

Table 3 Critical Depths for breakouts calculations for two borehole directions in each tectonic faulting regime, for case of hydrostatic fluid pressure λ=0.4 and σ_c = 50 MPa

	Hole axis	Av k_H	Av k_h	S/SB First Criterion	Depth Crit S/SB (km)	SB/U Second Criterion	Depth Crit SB/U (km)
					λ=0.4 σ_c=50 MPa		λ=0.4 σ_c=50 MPa
Normal							
	→ S_H		0.57	$(3 - k_h - 2\lambda) .27z \geq \sigma_c$	1.14	$(1 + k_h - 2\lambda) .27z \geq \sigma_c$	2.41
	→ S_h	0.87		$(3k_H - 1 - 2\lambda) .27z \geq \sigma_c$	1.39	$(1 + k_H - 2\lambda) .27z \geq \sigma_c$	1.73
Strike-Slip							
	→ S_H		0.71	$(3 - k_h - 2\lambda) .27z \geq \sigma_c$	1.24	$(1 + k_h - 2\lambda) .27z \geq \sigma_c$	2.04
	→ S_h	1.31		$(3k_H - 1 - 2\lambda) .27z \geq \sigma_c$	0.87	$(k_H + 1 - 2\lambda) .27z \geq \sigma_c$	1.23
Reverse							
	→ S_H		1.30	$(3 - k_h - 2\lambda) .27z \geq \sigma_c$	0.88	$(k_h + 1 - 2\lambda) .27z \geq \sigma_c$	1.23
	→ S_h	2.23		$(3k_H - 1 - 2\lambda) .27z \geq \sigma_c$	0.36	$(k_H + 1 - 2\lambda) .27z \geq \sigma_c$	0.74

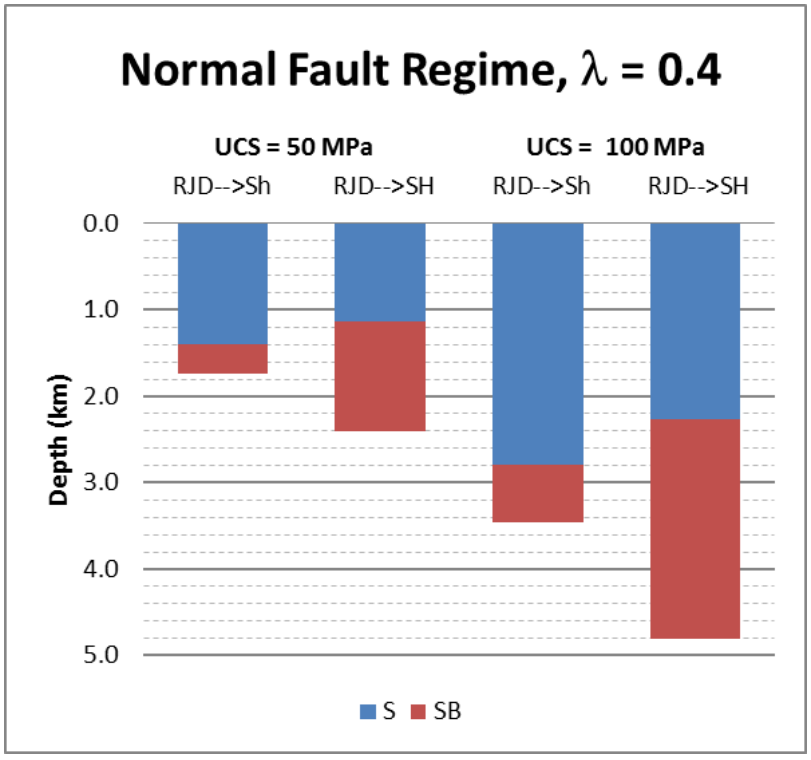

The SURE project has received funding from the European Union's Horizon 2020 research and innovation programme under grant agreement No 654662.

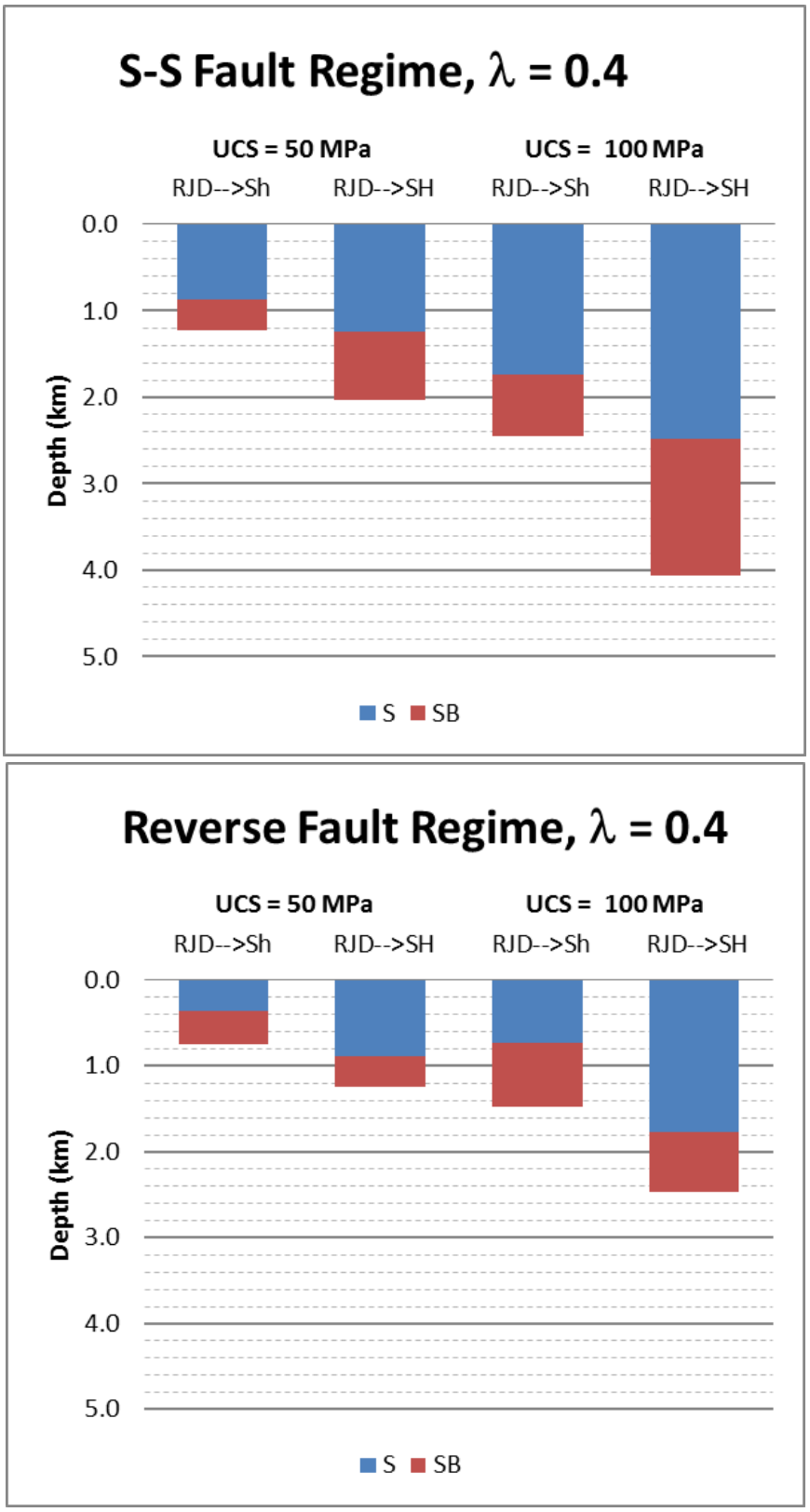

Figure 4. Depth to breakout (S/SB) and Collapse (SB/U) of RJD laterals: prediction plots applying k_h and k_H best fit Q-WSM database ratios from Zang et al., (2012), see Table 2; the three faulting regimes, two UCS rock strengths, two RJD directions (see Fig. 2).

The SURE project has received funding from the European Union's Horizon 2020 research and innovation programme under grant agreement No 654662.

The basis for the calculation of critical depths was given in Section 3.2 and is illustrated in Table 3. Fig. 4 covers a range of reservoir scenarios for the critical depths for all the three faulting regimes. The results in Table 3 can be seen plotted in the first two columns in Fig. 4 where only $\lambda = 0.4$ and UCS = 50 MPa were considered. For each critical depth calculated, the associated total in-situ stresses (S_v, S_H, S_h) can be readily recovered. For example the most critical condition and most fragile cases that will initiate SB/U i.e. likely total wall-rock collapse, for each faulting regime in the λ=0.4 and UCS = 50 MPa rock are:

Normal faulting regime: z = 1.731 km, S_v = 46.7, S_H = 40.7, S_h = 26.6 MPa
S-S faulting regime: z = 1.226 km, S_v = 33.1, S_H = 43.4, S_h = 23.5 MPa
Reverse faulting regime: z = 0.740 km, S_v = 20.0, S_H = 44.6, S_h = 26.0 MPa

The influence of tectonic regime is illustrated for RJD→ S_h where it is seen that the lateral becomes increasingly prone to breakouts (S/SB) and to collapse (SB/U) in shallower depths as consideration of the regime switches from Normal to Strike-Slip to Reverse. The trend is not so consistent for RJD→S_H as this presents a relatively higher stress ratio across the hole, making it more vulnerable in the Strike-Slip case than in the Normal case for breakouts. The trends for Reverse are quite severe – where relatively shallow depths are needed for prevention of breakout and instability.

The hole direction is very significant for the Normal Fault regime where S/SB breakout initiation for RJD→S_H is 1.14 km, while for RJD→S_h it is deeper at 1.39 km. However the contribution of S_H to a higher mean stress across holes with RJD→S_h means that Collapse instability (SB/U) may be only a little deeper at 1.73 km whereas for RJD→S_H it would be much deeper at 2.41.

The different criteria, signalling breakouts and signalling collapse, are only separated by a small depth increase in the RF case, whereas for NF the breakouts can begin at quite shallow depths but can tolerate much greater depths before collapse would be expected, due to the lower mean stresses generally. This is especially noted for RJD→S_H in RF and SS regimes. Drilling RJD→ S_H always allows much deeper jet-holes to be stable. However, for NF they are then less favourably orientated to intersect fractures and fulfil their function which is to intersect fracture permeability (see Fig. 2).

The theory is based on stress level comparisons with UCS so that doubling the UCS doubles the depth to S/SB and to SB/U transitional behaviour. The influence of UCS on depth to breakouts (S/SB) and on depth to collapse (SB/U), is illustrated for the Normal Fault regime in Fig. 5 (top, middle) for a range of k_h stress ratios and the depth to collapse is contrasted with the Reverse Fault regime in Fig. 5 (bottom). Consider now an igneous rock type such as granite or basalt with UCS of 200 MPa in a hot hard rock pilot geothermal reservoir project in which it is hoped that lateral jetting technology is successful in excavating holes. Collapse

The SURE project has received funding from the European Union's Horizon 2020 research and innovation programme under grant agreement No 654662.

phenomena at ~3 km is predicted if a Reverse Fault regime with WSM average k ratios were to exist at such depths (which is improbable) according to assumptions made here for $\lambda = 0.4$, RJD→S_h and $k_h = 2.25$. It is more likely that at such depths, there will be a Normal (or Strike-Slip) Fault regime in which case collapse behaviour may be supressed to at least 8 km, for an assumed k_h~0.7. However, it is uncertain whether for all rock types especially tough brittle rock, M-C predictions are appropriate as tensile splitting may be the main early failure mode. Tensile crack initiation by radial extensional strain splitting at tangential stresses significantly below UCS values was proposed and discussed by Stacey (1981); Shen (2008); Shen and Barton (2018).

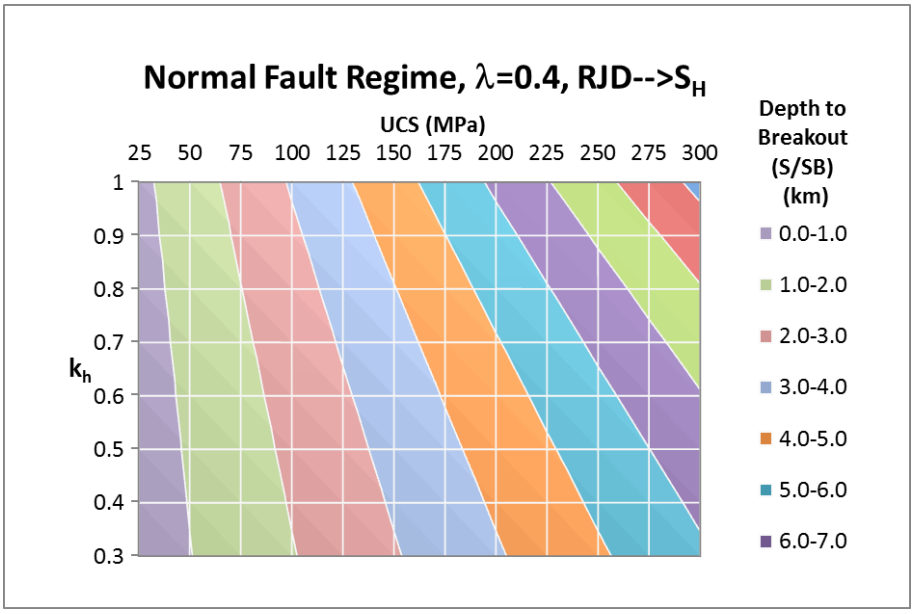

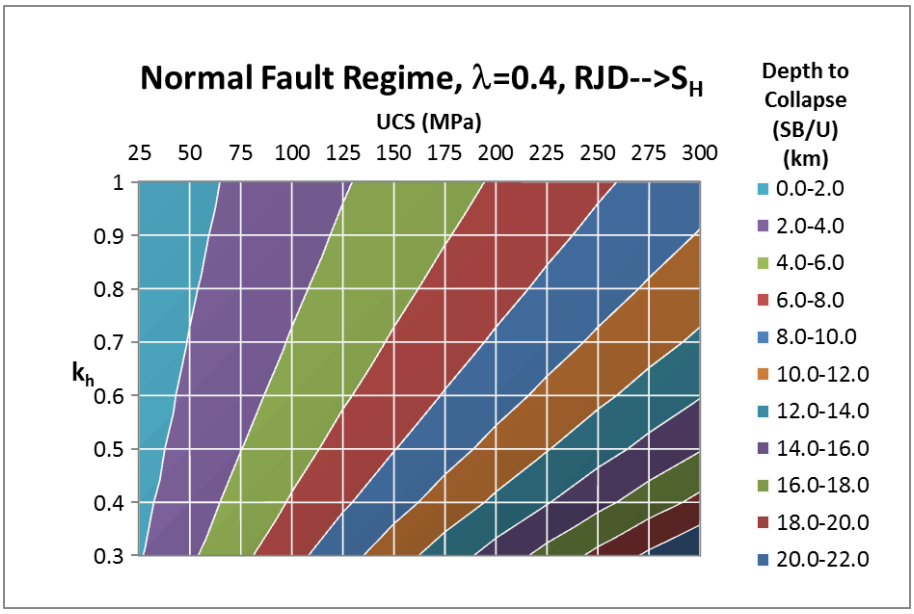

The SURE project has received funding from the European Union's Horizon 2020 research and innovation programme under grant agreement No 654662.

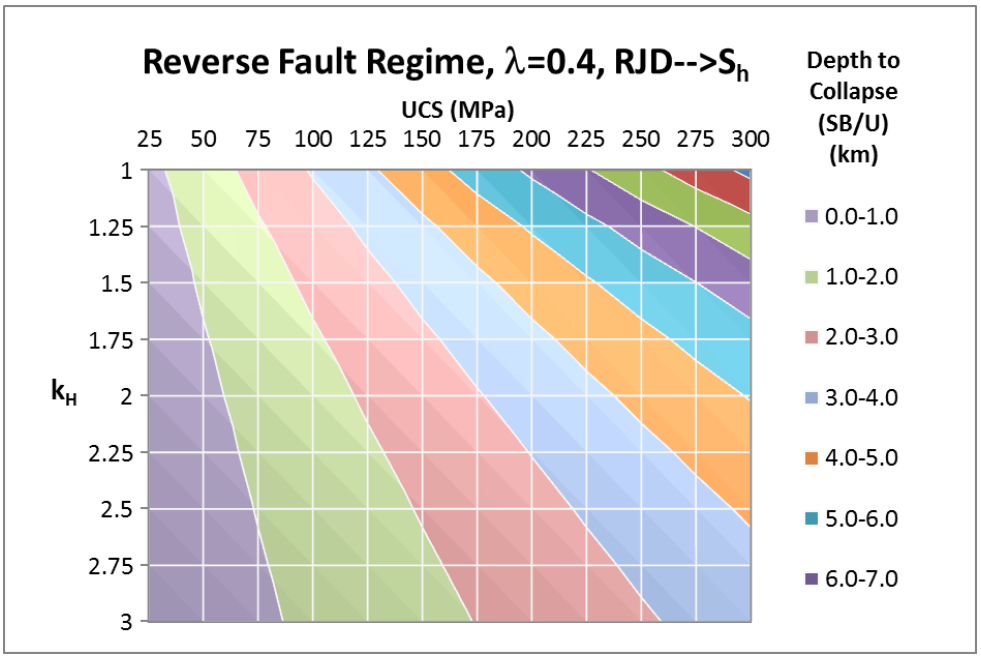

Figure 5. Depth to Breakout (S/SB) and to Collapse (SB/U) presented as contour plots for variable UCS, k_h, k_H and faulting regimes: (top) Normal Breakouts (S/SB), (middle) Normal Collapse (SB/U) and (bottom) Reverse Collapse (SB/U).

Given the great uncertainty of the most reasonable in-situ stress magnitudes, further sensitivities to the transitional depths as a function of k_h and k_H have been plotted in Fig. 6 for the three regimes, with a hydrostatic pressure gradient (λ=0.4) assumed. This enables a fuller understanding of the consequences of any given true horizontal to vertical in-situ stress ratio as this may vary significantly from the global average values illustrated in Fig. 4. Consider for example, an extreme case with a UCS of 50 MPa, k_H of 3.0 in the Reverse Faulting regime; complete collapse is predicted at 600 m (Fig. 6 bottom).

The U threshold condition (SB/U), signalled by depths at which the breakout angle is likely to exceed 90 degrees in conventional drilling is often associated with lack of arch support, hole widening in all directions and washouts. As RJD laterals aim to exploit horizontal drilling, gravity cannot assist in removal of wall collapsed fragments as easily as for conventional vertical boreholes. However, not much is known about the ability of high water-jet pressures to comminute and transport/convey back through the annulus the suspended fines, fragments and wall rock that collapses during the excavation phase. How much drilling depth and wall stress increase can be tolerated above that needed to initiate breakouts before arch support loss, run-away collapse and/or equipment mal-functions would be expected? remains an open question. Experience from RJD operators will be invaluable to answer this question. This is of particular importance as any sustainable increase in the size of the jetted hole, the conduit for fluid flow, will enhance the heat recovery from the lateral jet-hole. For geothermal wells which are generally producing and injecting at high rates (100-200 m^3/hr), pressure drop in the jetted laterals reduces their impact. Modelling suggests that increasing the effective

The SURE project has received funding from the European Union's Horizon 2020 research and innovation programme under grant agreement No 654662.

diameter has an approximately linear impact on increasing injectivity index (Peters et al., 2019).

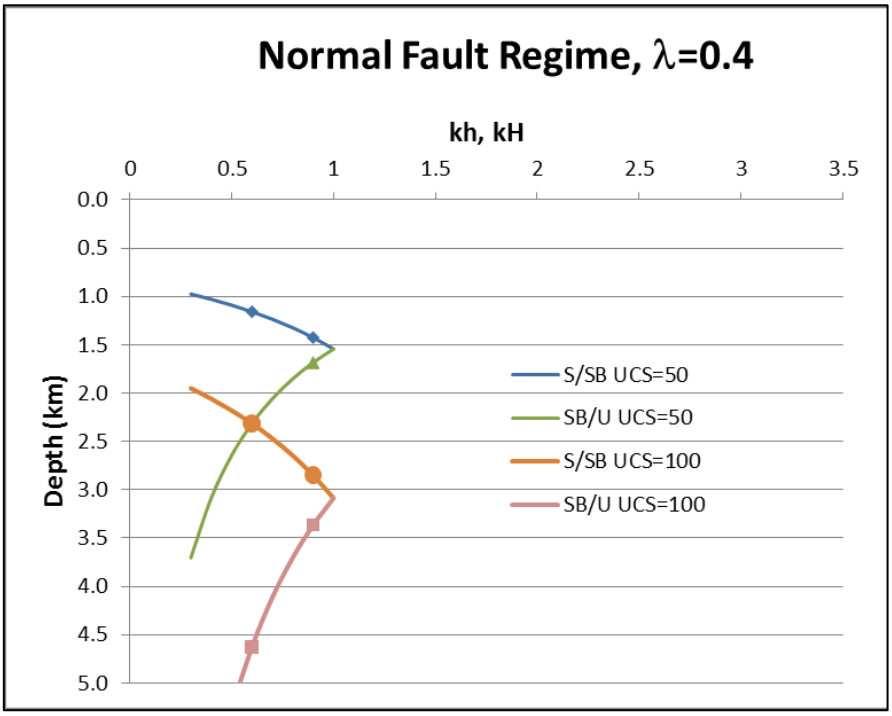

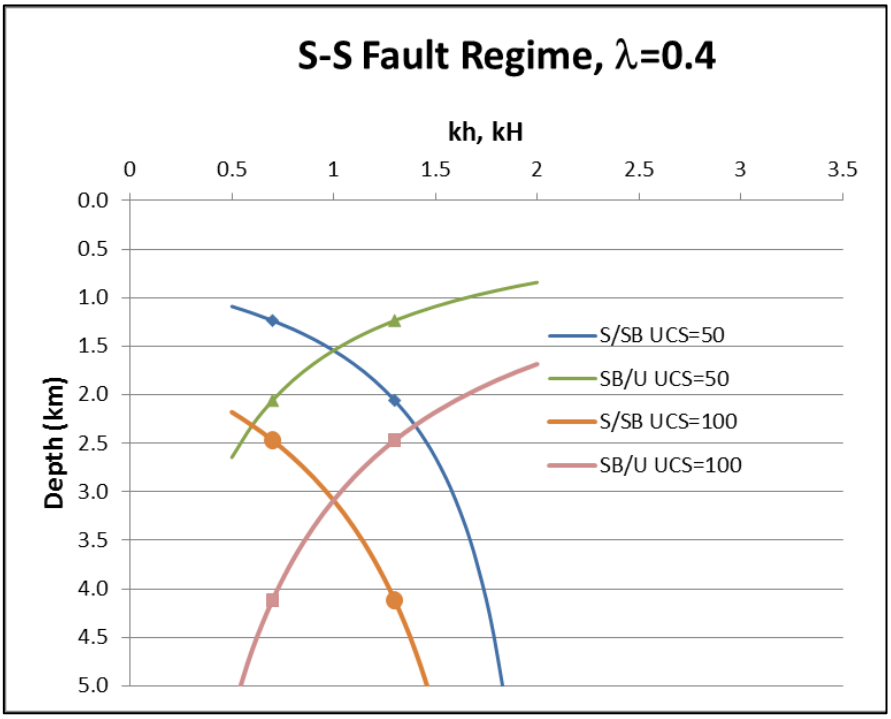

The SURE project has received funding from the European Union's Horizon 2020 research and innovation programme under grant agreement No 654662.

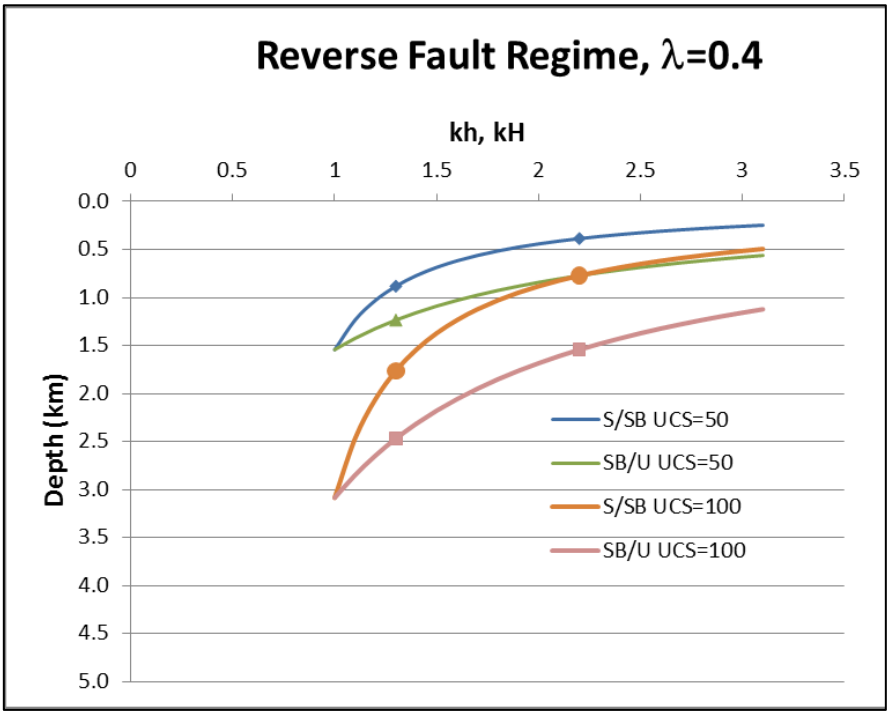

Figure 6. Depth to initiation of breakouts (S/SB) and initiation of collapse (SB/U) curves for a range of hypothetical k_h and k_H values, together with their best-fit values from the Q-WSM database (symbols), for different faulting regimes, two UCS values and λ=0.4.

It is also important to recognise the limitations of this simple analysis which does not consider the progressive deformation process of wall collapse, or the resultant changes in local wall stress with distance from the eroding front. In reality, the jet-hole profile evolves to the 2D plane strain case a certain time after the jet head passes through. Each piece of rock ahead of the jet that later becomes wall rock material after the hole passes through will experience a specific stress state history ending with its highest differential stress state given by the 2D Kirsch solution. This 2D solution was considered sufficient for assessing the stability of wall rock in cylindrical jetted holes. A simple Mohr-Coulomb failure model that ignores the intermediate stress was assumed which enabled shear failure criteria based on UCS to be applied. Extremes for the intermediate principal stress ($\sigma_1 \approx \sigma_2 > \sigma_3$ and $\sigma_1 > \sigma_2 \approx \sigma_3$) were not considered and having applied M-C, intermediate stress has been implicitly assumed not to play a significant role. In the next part of the report, the evolution of breakouts and collapse behaviour will be modelled using the FEMDEM code, Solidity, (e.g. see Guo et al., 2017; Lei et al., 2017). The applicability of the wall-rock stability prediction presented in this part (Section 3) will be examined.

3.4 Conclusions

Conventional vertical borehole breakout stability analysis based on Kirsch equations can be readily extended to open horizontal holes and generalised for the three tectonic faulting regimes to provide guidance on depth to breakout for jetting parallel to S_{Hmax} or S_{hmin}. The

The SURE project has received funding from the European Union's Horizon 2020 research and innovation programme under grant agreement No 654662.

transition from stable cylindrical wall rock to stable with initiation of breakouts is presented and illustrated as a *first criterion* for ultimate strength of open jetted boreholes.

In Radial Jet Drilling (RJD) application to geothermal energy exploitation, any increased cross-sectional area in a jet-hole that remains stable is an advantage for enhanced heat recovery so break-outs may not be problematic. Reservoir engineers are well aware that in certain combinations of local conditions, wall integrity may be compromised for a large part of the circumference of the original hole's diameter and measures based on mud weight calculations are applied to prevent wash-outs and run-away collapse for cased well-bores.

An expression for a *second criterion* is presented for this transition to unstable collapse of open holes based on when breakout angles can be expected to exceed 90 degrees, a condition strongly dependent on the mean of stresses acting perpendicular to the hole. This leads to a wide variety of possible 'windows of opportunity' whereby a given in-situ stress field should allow stability to remain so that stable and enlarged holes that are unlikely to collapse can still be exploited. An intriguing question to address is then – what mechanisms take over the failure process leading to jet-hole arch support failure and possible run-away collapse when stresses first exceed those for which holes with already advanced breakouts just remain stable.

Simple equations calculating stable depths for open horizontal cylindrically jetted holes are presented together with formulae and illustrative charts using average horizontal to vertical stress ratios from the Quantitative World Stress Map database for the three different Faulting regimes. The effects of UCS, direction of jetting, k_h and k_H are extensively examined.

The SURE project has received funding from the European Union's Horizon 2020 research and innovation programme under grant agreement No 654662.

DOI: 10.2312/GFZ.4.8.2019.009

4 Numerical Modelling of Jet-hole Stability

4.1 Introduction

In this section numerical modelling methods are introduced and applied to the study of jet-hole stability. The modelling study presented here is linked closely to an experimental study of jet drilling into triaxial stressed sandstone rock blocks (TUDelft, WP4). The breakout phenomena and geometry of the experimental jet-holes observed are reported here in order to discuss and strengthen the findings of the numerical modelling study. Two numerical modelling methods are applied, classical finite element analysis (FEM) and the hybrid finite-discrete element method (FDEM). The modelling described first uses an elastic FEM analysis. The continuum-based FEM modelling is used here to elaborate upon the local stress field to be expected in 3D in both idealised cylindrical jet-holes and in the irregular jet-hole geometries actually found, and as a consequence of jetting into different in-situ (i.e. far-field) stresses. To model rock behaviour when stresses exceed strength in the wall-rock surrounds of the jetted hole, the hybrid finite-discrete element method (FDEM) is very well suited. This can simulate the growth of fractures and has the potential to confirm the predictions of Section 3 and add further understanding and prediction of when and how a jet-hole can be expected to enlarge and collapse.

The modelling research (Section 4) is organised as follows. Section 4.2 begins with a brief background to the FEM software and elaborates on the less well-known FDEM methods and the in-house code ***Solidity*** employed in this work which leads into a final section describing the development in this project of a new tool that couples an FEM solver to an FDEM solver in a manner that solves the problem of unwanted stress waves when FDEM is applied unaided (Section 4.2). The results of true triaxial laboratory jetting tests are then highlighted (Section 4.3). First, FEM results are compared with experimental results using normalised stress parameters designed to highlight regions expected to be near to failure (Section 4.4). Second, using the new tool FDEM results are reported showing initiation of fractures and their evolution associated with breakout development in stress fields tested in the laboratory (Section 4.5). The in-situ stress conditions given by an average horizontal to vertical stress ratio of 0.57 are investigated to compare with the predictions of depth for onset of breakouts and final collapse calculated from the Kirsch solution in Section 3. There follows a discussion in Section 4.6.

4.2 Modelling Methods

4.2.1 FEM Analysis

A simple elastic analysis of the stress field around cylindrical holes based on Kirsch solutions of the 2D problem where stress levels are compared with criteria of rock failure goes a long way to predicting wall-rock stability, as seen in Section 3. To explore the special case of radial jet-hole stability, a full 3D elastic solution is informative. A finite element method (FEM) solver in MATLAB has been adapted and applied to analyse the wall-rock stress state using

The SURE project has received funding from the European Union's Horizon 2020 research and innovation programme under grant agreement No 654662.

the X-ray CT geometries of jetted holes. Different far field stress boundary conditions for rock with given Young's modulus and Poisson's ratio elasticity coefficients can then be considered.

Based on the experimental setup (Bakker et al. 2018), a 300 mm edge cube was created with the CAD software Rhinoceros. Different hole shapes have then been subtracted from the cubic volume. The resulting geometries were then imported into MATLAB and the effects of applied triaxial stresses simulated with the 3D FEM PDE solver in MATLAB. Here we illustrate the method using in-situ stresses in a plane-strain model: σ_v on the top edge, σ_h on the left edge and roller constraints on the right and bottom edges. The resulting three-dimensional displacement field is shown in Fig. 7. The displacement, strain and stress fields are computed with a static analysis and an implicit solver. The results can be used to interpolate boundary conditions of two-dimensional plane-strain FEM and FDEM simulations for a given set of elastic moduli.

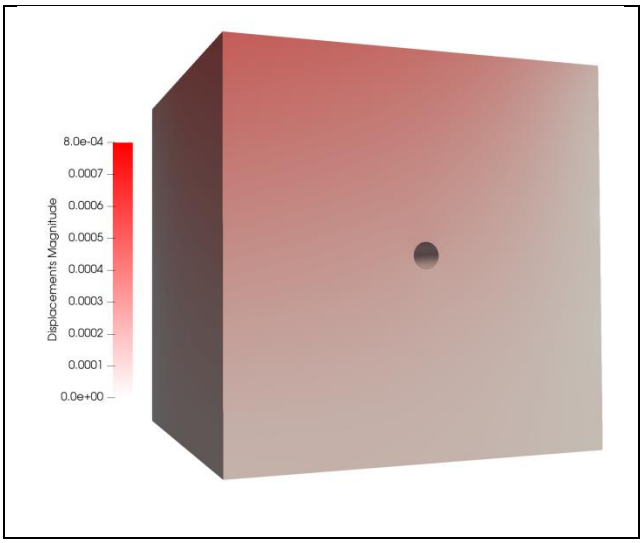

Figure 7: 3D model of an idealised cylindrical jetted borehole.

4.2.2 Boundary element code FRACOD - analysis review

Progressive fracture development modelling in the context of boreholes and tunnels has also been reported by Shen and co-workers, using a boundary element code FRACOD (Shen et al., 2014) incorporating displacement discontinuity elements and fracture mechanics criteria with Mode I and Mode II energy release rates, tensile strength, cohesion and internal friction angle properties. The model generates predictions of fracture initiation and propagation. Breakout fracture predictions using FRACOD for tunnel applications from Shen and Barton (2018) are shown in Fig. 8. In terms of the simple criterion (S/SB) for initiation of breakouts presented in Section 3, ($\sigma_{\theta max}$ > UCS), for the 1 km in-situ stress, $\sigma_{\theta max}$ is 125 MPa while UCS = 165 MPa, so conditions should not show breakouts, however deep breakouts are numerically predicted to occur according to the FRACOD model in Fig. 8 (left). For the weaker rock and at 2 km

The SURE project has received funding from the European Union's Horizon 2020 research and innovation programme under grant agreement No 654662.

depth, more severe fracturing is implicated by the FRACOD simulation results with fractures definitely exceeding 90 degrees of breakouts and tensile spalling completing a predicted 360 degrees of wall damage. This degree of failure agrees with the second simple criterion (SB/U) for collapse (when $\sigma_{Hmax} + \sigma_V > UCS$). However, in these fracture breakage simulations it is not clear to what extent the model includes certain potentially important processes. For example, the frictional interactions of the sliding surfaces of displacing newly formed propagating fractures and the transient effects of stress relaxation may not be captured in the progressive deformation, as the contact interactions are not naturally captured. Wing cracking often associated with tips of shear fractures are not shown here. We therefore turn to the FDEM code Solidity for the transient dynamic evolution of structural damage to the jet-hole wall.

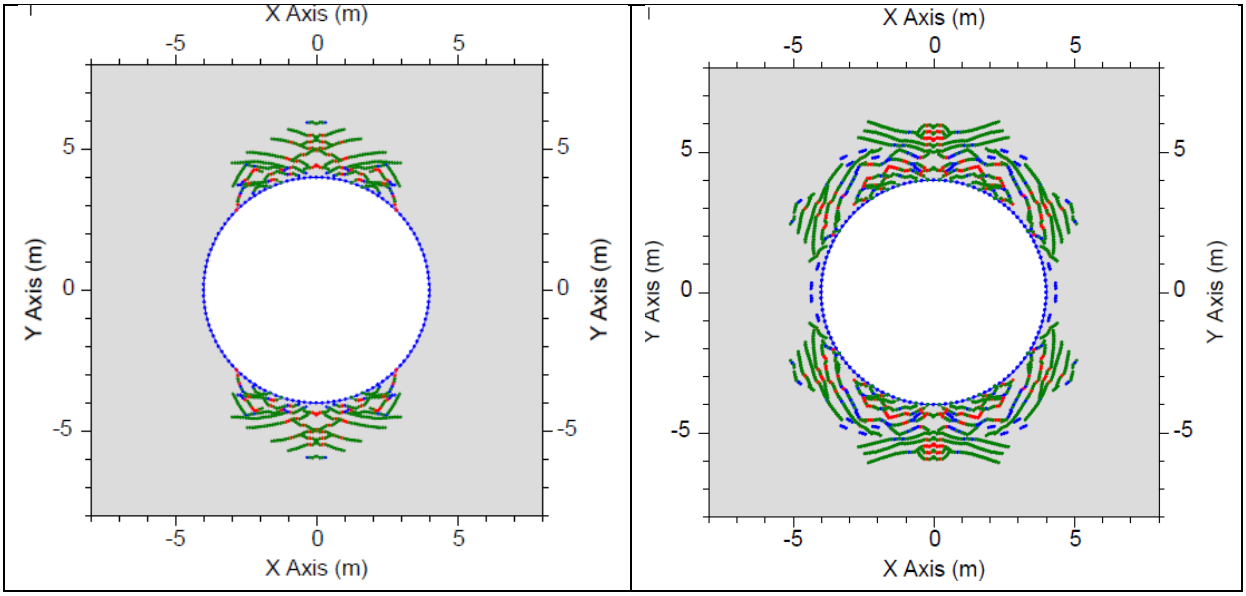

Figure 8. Simulation of fracture patterns generated by Boundary Element Code, FRACOD (Shen et al., 2014) as reproduced in the paper by Shen and Barton (2018). The blue and red fractures are Mode I tensile, the green fractures are Mode II. Boundary stresses σ_{Hmax} = 50 MPa and σ_v = 25 MPa i.e. Reverse Faulting regime, Left: in strong rock with UCS = 165 MPa for a depth of 1 km. Right: in weaker rock with UCS = 82 MPa for a depth of 2 km, σ_{Hmax} = 100 MPa and σ_v = 50 MPa.

4.2.3 FDEM Analysis

The hybrid finite-discrete element method (the original abbreviation for this hybrid method 'FEMDEM' has in recent years been shortened by many authors to 'FDEM') combines the finite element analysis of stress/deformation history with the discrete element solutions of transient dynamics, contact detection and interaction. For rock masses or intact blocks with or without pre-existing cracks, in such a discontinuum modelling scheme, the internal stress field of each discrete matrix block is calculated by the FEM solver, (note in this case an explicit solver is used for the transient dynamic effects of stress waves and smaller time steps are required) while the translation, rotation and interaction of multiple rock blocks are tracked by the DEM algorithms. Pre-existing fractures in rocks are treated as the internal boundaries of rock volumes. The FDEM approach also provides a natural means to model the transitional

The SURE project has received funding from the European Union's Horizon 2020 research and innovation programme under grant agreement No 654662.

behaviour of brittle and quasi-brittle materials from continuum to discontinuum (i.e. fracturing processes) by integrating fracture mechanics principles into the formulation. The two most commonly used FDEM formulations are the commercial software ELFEN (2011) which is partially discontinuous in that joint elements are inserted only where pre-existing fractures and new fracturing is occurring, and an opensource platform Y-code (Munjiza, 2004) which uses a fully discontinuous mesh with joint elements embedded between the interfaces of all finite elements (i.e. along fractures and inside intact domains). The Y-Code has led to numerous versions emerging, notably the one developed by a collaboration between Queen Mary University and Los Alamos National Laboratory, (e.g. Rougier et al., 2014), the Y-Geo code by Toronto University (e.g. Mahabadi et al., 2012) and the Solidity platform developed by Imperial College London. FDEM code, Solidity (formerly, VGeST and VGW), (e.g. see Xiang et al., 2009 and for fracture modelling in FDEM, see Guo et al., 2017; Lei et al., 2017b, Latham et al., 2013). The deformation of the bulk material is captured by the linear-elastic constant-strain finite elements with the impenetrability enforced by a penalty function and the continuity constrained by a constitutive relation. The interaction of matrix bodies through newly formed discontinuity interfaces on either side of a fracture is simulated by the penetration calculation (Munjiza and Andrews, 2000). The brittle failure of intact materials is governed by both fracture energy parameters (for mode I and mode II failure) and strength properties (e.g. tensile strength, internal friction angle and cohesion). A numerical calibration can be conducted to achieve consistency between the input material strength parameters and simulated macroscopic response (Tatone and Grasselli, 2015), however this is not a straightforward process. For example, fracture energy release rate values used in simulations to produce self-consistent calibrations of specimen failure may need to be different from rock representative material properties obtained directly from laboratory fracture toughness experiments. For detailed reviews that place hybrid FDEM methodology in a rock mechanics context, see Lei et al., (2017a), Lisjak and Grasselli (2014).

Currently, there are two main challenges (further discussed below) for the application of Solidity's FDEM to jet-hole stability prediction. First, progressive circular hole removal (by jet action) is not easy to represent realistically in an efficient series of modelling steps. Second, very small time-steps and fine mesh requirements of FDEM are needed to avoid unrealistic shock wave effects when modelling the application of stresses at the boundaries of an otherwise unstressed rock domain. This leads to excessive run times.

To elaborate on the first challenge; as with excavation of tunnels, the evolution of the stress history of rock elements in the jet-hole wall varies spatially and in time. The rock material, initially in equilibrium under far field stress is gradually affected by the de-confinement caused by the approaching excavation and eventually after the excavation front has gone through, the wall rock is left in a stress field approximated well by the 2D plane strain assumption if more than about two diameters behind the jet-hole's advancing front (Eberhardt 2001). To model the 2D stresses that surround the hole that drive breakout development and

The SURE project has received funding from the European Union's Horizon 2020 research and innovation programme under grant agreement No 654662.

possibly collapse, one option is to apply stress de-confinement phasing. The excavation modelling starts by achieving a computational domain of rock with far field in-situ stresses and the rock in equilibrium, and no hole. It then relaxes a circular domain representing the hole by gradually ramping down the stiffness at a rate that avoids sudden shocks. This is followed by circular material removal. The loss of confinement with raised hoop stresses renders the wall-rock vulnerable to fracturing and fragment/block motion into the excavation. See for example the FDEM modelling of excavation damage during tunnelling by Lei et al., (2017b).

An alternative loading history, potentially easier to apply, but possibly less valid is to consider that the stability behaviour can be approximately captured with a computational domain of rock with a pre-existing appropriately sized small circular hole at its centre. The stresses at the domain boundaries are ramped up linearly from zero towards the state of the far field stresses of interest. Any signs of fracture failure with breakouts but with a lack of total collapse when the final stress state is reached would suggest a viable stable hole for the in-situ stress and rock type in question. In this work, we adopt the latter alternative stress history although it is planned in future work to investigate the differences in results between the two methods.

Turning to the second challenge, the consequences of the explicit FDEM solver methods with their small time steps mean that run-times are impractically long if the ramping up of the stresses from zero is performed slowly enough to avoid artificial stress wave transients. The problem is that any simulation that applies steady displacement or ramping stress conditions at the domain boundary will tend to generate stress waves that will have significant amplitude even with quite low boundary displacement or stress ramping rates, meaning the deformations are not quasi-static and premature fracturing may result.

4.2.4 New coupled protocol tool: implicit FEM – explicit FDEM

The aim is to generate a suite of boundary condition tools for combined finite-discrete element (FDEM) application to laterals with axial (cylindrical and irregular) holes jetted into triaxially stressed reservoir rock masses. The tool would then be suitable to enable FDEM modelling of the stress state and potentially the fracture and breakout development, both examining true-triaxial stress conditions under which water jet-holes were drilled and found to be stable with well-developed breakouts (WP4 and WP5), and for generic application to modelling reservoir field scenarios.

To prevent shock wave effects without undue extension of run times, a novel approach is proposed. The background known elastic solution for displacements of all nodes, not just those at the boundary, guides the input to successive steps of the FDEM solution. This prevents locally steep stress gradients and wave transients. These are calculated e.g. by MATLAB using elastic FE analysis over the full domain. For implicit FE solutions, large displacement increments are acceptable. A coupling procedure that cycles between FEM and

The SURE project has received funding from the European Union's Horizon 2020 research and innovation programme under grant agreement No 654662.

FDEM codes was devised. The FEM part feeds the correct large increment displacements to successive FDEM sub-cycles that update possible elastic and inelastic fracture deformation including shear displacements on fractures.

A protocol combining the FEM in MATLAB with Solidity's FDEM has been developed in this project to enable large regions of purely elastic response to be captured with implicit elastic FEM solutions for the entire domain's displacement field. This is performed by ramping relatively large stress increments at the boundaries of the domain and computing new elastic response displacement fields. The new displacement field of the FEM model at the boundaries is interpolated on the FDEM mesh and used as a constraint for the boundary nodes in the next FDEM step. The variation in the displacement between field stress increments in the FEM model is also interpolated in the FDEM mesh and used as a nodal 'push displacement' for the rest of the simulated domain. This defines the new input to the FDEM solver which runs for a pre-set time interval sufficient for equilibrium to be reached, whether the deformation is elastic or involves brittle fracture, shearing, crack opening, fragmentation etc. The nodal 'push displacement' applied to the interior nodes of the mesh acts as a preconditioning for the FDEM solver. In this way the solver starts each computation with an updated nodal displacement field that is already close to the equilibrium configuration for the given boundary conditions. Moreover, the 'push displacement' field incorporates the portion of the nodal displacements that is due to the elastic deformations of the finite elements of the mesh. In this way, only the small increment in the displacement due to the joint-elements' artificial compliance has to be computed by the FDEM solver in each iteration in order to find the equilibrium configuration. These displacements, which are due to the extremely small overlapping of the FDEM elements, are often at least one order of magnitude smaller than the elastic displacements, depending on the penalty parameters employed in the simulation. As introduced above, this has also the effect of reducing the propagation of stress waves in the domain generated by the boundary conditions.

Another advantage of this procedure is that it does not influence the preliminary crack developments during loading. In the FDEM model, cracks can only propagate between the edges that elements of the mesh have in common, i.e. element boundaries. At the beginning of the simulation, the two couples of nodes of any adjacent edge that two elements have in common will share the same coordinates. The collection of coordinates of these two couples of contiguous nodes is commonly referred as a joint-element. The 'push displacement' applied to the nodes of the mesh is calculated based on the initial coordinates of the nodes of the mesh. For this reason, any couple of nodes of the adjacent edges of the elements of the mesh will receive the same 'push' and no relative displacement is applied between the edges of the mesh. This ensures that the opening of the joint-elements is not influenced by the applied displacements during each loading step.


The SURE project has received funding from the European Union's Horizon 2020 research and innovation programme under grant agreement No 654662.

Each subsequent FEM step is run to obtain the new displacement constraints to be applied throughout the domain – not just at the boundaries. These displacements are then passed as inputs to restart the FDEM solver which models the time marching response. The methodology is illustrated with an example in Fig. 9.

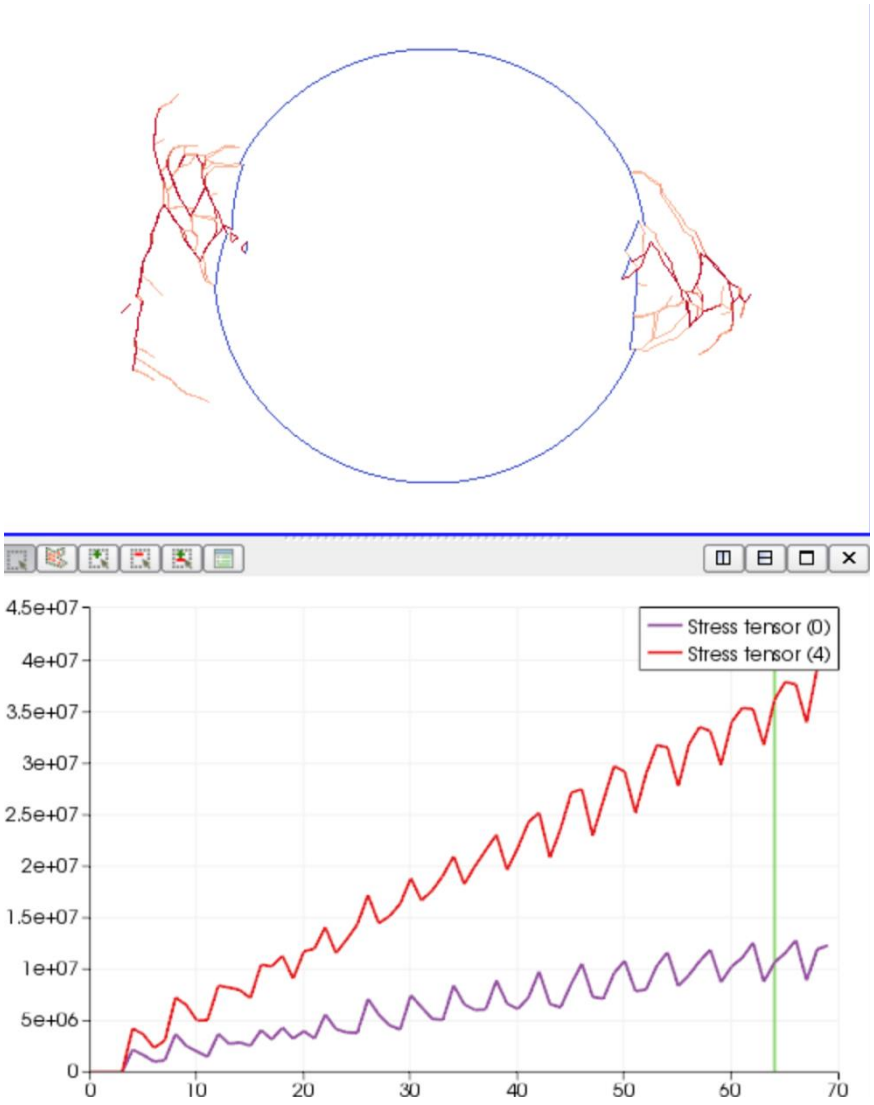

Figure 9. FEM/FDEM protocol and illustrative results. Top: 20 mm holed 300 mm square specimen with breakout deformation features for load condition shown by green line below. Bottom: Stress history at a sampling point located half way between the bottom left corner of the domain and the centre of the hole. The block is loaded with boundary ramping stress increments of 2:0.67 MPa each, giving a ratio of 3:1 vertical to horizontal.

4.3 Stability of laterals from laboratory jetting tests under true-triaxial stresses

Jet drilling experiments with an 18 mm rotating nozzle (Fig. 1) were performed in TUD laboratories on 300 mm cubes of Gildehaus Sandstone (of Bentheim formation) under several states of true triaxial boundary conditions. Tests were originally designed to investigate

The SURE project has received funding from the European Union's Horizon 2020 research and innovation programme under grant agreement No 654662.

factors affecting rates of penetration (WP5) but revealed a wealth of data relevant to lateral hole wall stability and the objectives of task 7.2. The apparatus can apply a maximum load of 3500 kN in each orthogonal direction (38.9 MPa with 300x300mm area). Strain is calculated from displacement measurements (LVDTs) placed parallel to the loading directions. Jetting initiated at the centre of one of the cube-faces where a metal nut was glued into the rock, such that a feed-trough pipe could be mounted. This pipe also enabled the capture of outflowing water and debris for further analysis. Pore pressure in the rock could not be maintained due to edge effects (pistons should not touch each other). It is therefore assumed that the pore pressure is nearly atmospheric throughout testing, except locally where the jets impinge. The geometries of the excavated holes were determined using a (medical grade) X-ray CT scanner as installed at the TU Delft GSE laboratory, and subsequent 3D image processing using commercially available dedicated software (Avizo, Thermo Fisher). It is assumed that the geometric form (Fig. 10), represents the equilibrium state of each hole at the moment drilling action was terminated prior to unloading the test rig applied stresses and no further inelastic deformation was caused by unloading the samples. Geometric variations of the resulting jetted advancing front and side wall can be compared for example with an idealised smooth wall 18 or 20 mm cylindrical hole that might be anticipated for an 18 mm rotating nozzle.

For a preliminary assessment of the stability of the three jetted holes shown in Fig.10, the key Kirsch equation predictions (S/SB and SB/U in Section 3) for whether breakouts or collapse should initiate assuming cylindrical holes for the three true triaxial state jetting tests are given in Table 3. The calculations indicate that the low isotropic stress in JO3 is very far from either breakout initiation or wall collapse. Both JO4 and JO2 can be expected to have well developed breakouts given that the values are well in excess of 1. The value 1.887 compared with 1.509 suggests a more deeply developed breakout would be expected for the higher stress anisotropy in JO2 as confirmed by the actual cross sections observed in Fig. 10. Column 4 indicates that the wall rock in both JO4 and JO2 would be equally likely to remain intact as the exceedance value for the collapse criterion based on mean stress, Eq (6), is significantly less than 1 and is equal to 0.755 in each case.

The objectives of the TUD experiments performed in WP4-5 included to examine the effects of in-situ stress magnitude and orientation on the overall jetting performance (i.e. rate of penetration) as well as to jet into fractures / voids to study potential curving effects. However, we restrict reporting to consideration of an assumed 2D stress field independent of stress in the hole axis (y) direction. Moreover, regardless of the stress conditions of each experiment, the resulting jetted borehole was straight. Variations along the borehole axis are only evident at the furthest leading edge, where the back-thrusters (see Fig. 1) have not reached. Here, at the borehole tip, the borehole is generally circular and narrower. Fig. 10 shows the distinctive jet-hole geometry responses. The breakouts in J04 are well developed in the direction aligned with the minimum stress (10 MPa) but hole widening is also surprisingly well developed in the direction aligned with the maximum stress (30 MPa). This could be associated with nozzle


The SURE project has received funding from the European Union's Horizon 2020 research and innovation programme under grant agreement No 654662.

vibration effects. The J02 breakouts appear more confined to a smaller breakout angle but are penetrating deeper. The rock block with its exact jet-hole excavation geometries can be represented with a computational mesh as shown in Fig. 10 (bottom) e.g. as required for further stress analysis. Both 2D and 3D elastic FEM considering known boundary in-situ stresses together with strength and deformability properties of Gildehaus Sandstone (Table 2) are presented in Section 4.4.

Table 3. TUD's true triaxial test conditions in the plane normal to the hole together with calculated measure of stress/strength exceedance for Stable Breakout initiation (column 3) and for Unstable wall-rock collapse (column 4) according to the Kirsch solution and analysis in Section 3, assuming Gildehaus Sst UCS of 53 MPa.

Test Jetting	$\sigma_\theta = 3\sigma_{max} - \sigma_{min}$ MPa	σ_θ/UCS SB	$(\sigma_{max} + \sigma_{min})$/UCS U	σ_{max} MPa	σ_{min} MPa
J03	10	0.189	0.189	5	5
J04	80	1.509	0.755	30	10
J02	100	1.887	0.755	35	5

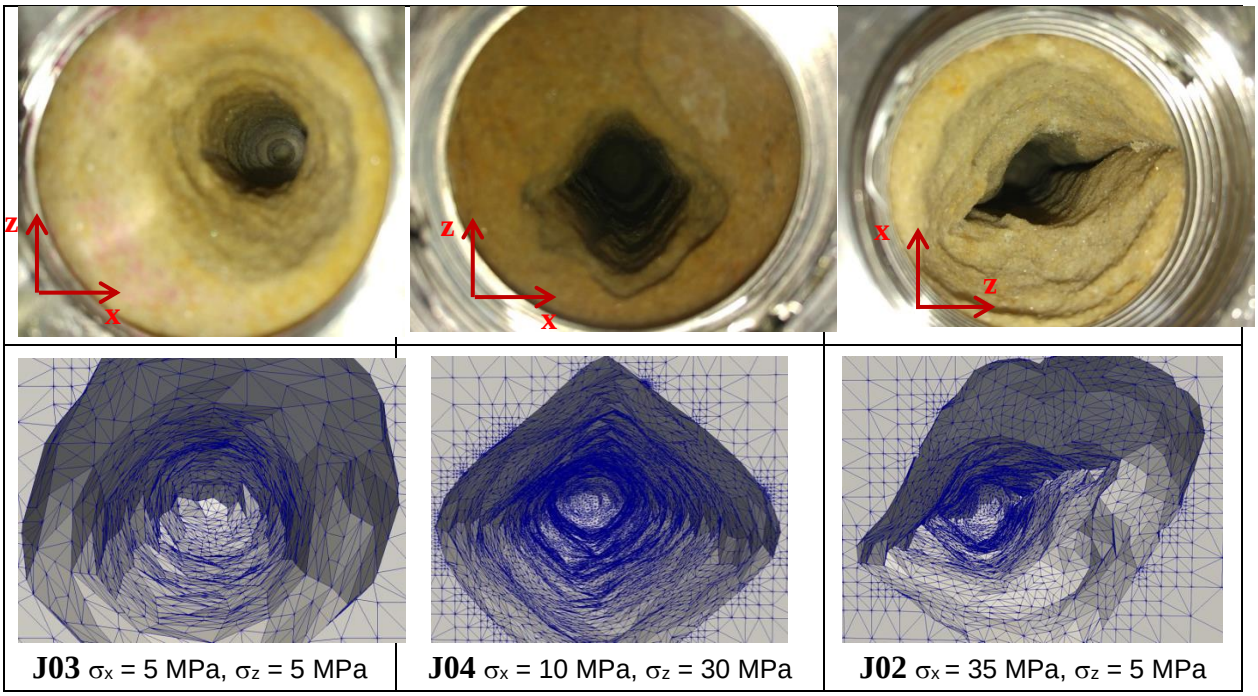

Figure 10. Top: Wall rock breakdown and break-out responses to rotating nozzle jet drilling in true triaxial stress conditions (from results of TUD tests, WP4-5). Metal threaded access diameter is ~ 60 mm, giving circular view of sandstone and jet hole. Bottom: X-Ray CT scan details of hole geometry visualized down hole including 3D surface mesh. Jetting tests performed at TUDelft by Richard Bakker (TUDelft) and Simon Hahn (GZB) for WP4 and WP5, X-Ray CT Avizo data from TUDelft.

The SURE project has received funding from the European Union's Horizon 2020 research and innovation programme under grant agreement No 654662.

4.4 FEM Results - Stresses around cylindrical jetted and irregular shaped boreholes

4.4.1 FEM analysis of stress for a cylindrical hole

Fig. 11 indicates that conditions for JO2 (7:1 ratio) would be likely to trigger tensile failures in the direction of maximum compressive stress, but not in the lower stress ratio case for JO4 (3:1 ratio). Signs of the existence of such tensile cracking will be investigated in microstructure examination of the jetted specimens in future work. Shear failure conditions are exceeded in positions predicted by the Kirsch solution (Fig. 3) and to greater depths into the wall for JO2, as borne out by the experiments.

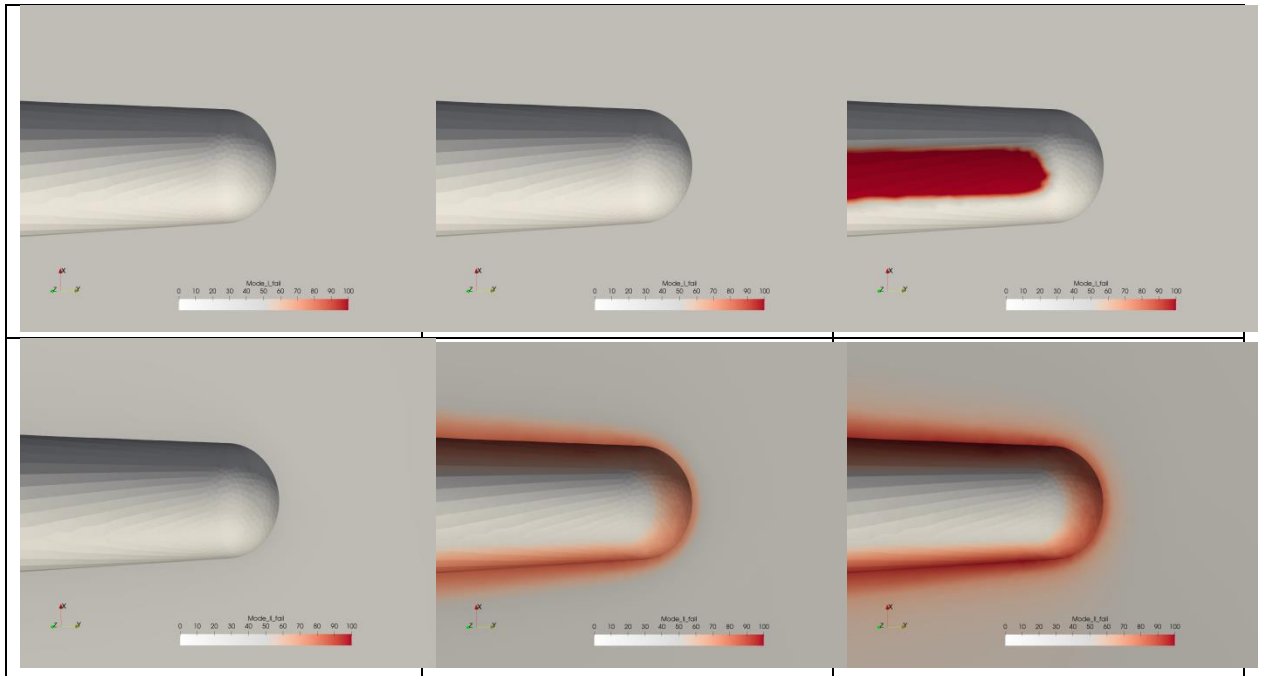

Figure 11. FEM analysis of 3D stress field for cylindrical hole with hemispherical end. Stress magnitudes shown as vertical slice through borehole and on internal wall surfaces. The three cases of triaxial in-situ boundary stresses used in experiments are presented. Stress level is shown normalized with respect to tensile strength as % of tensile stress required for tensile Mode I failure (top) and as % of the differential stress required for (Mohr circle with same mean stress to touch failure envelope for) shear Mode II failure (bottom) for Gildehaus Sandstone properties. X-Ray CT Avizo data from Richard Bakker, TUDelft.

The 2D FEM analysis in Fig. 12 presents numerical simulation results that are very close to the analytical Kirsch solutions based on far field stresses at infinity, (see also Table 3) as the 300 mm sides where the boundary stress is applied are relatively far away from the 20 mm diameter hole.

The SURE project has received funding from the European Union's Horizon 2020 research and innovation programme under grant agreement No 654662.

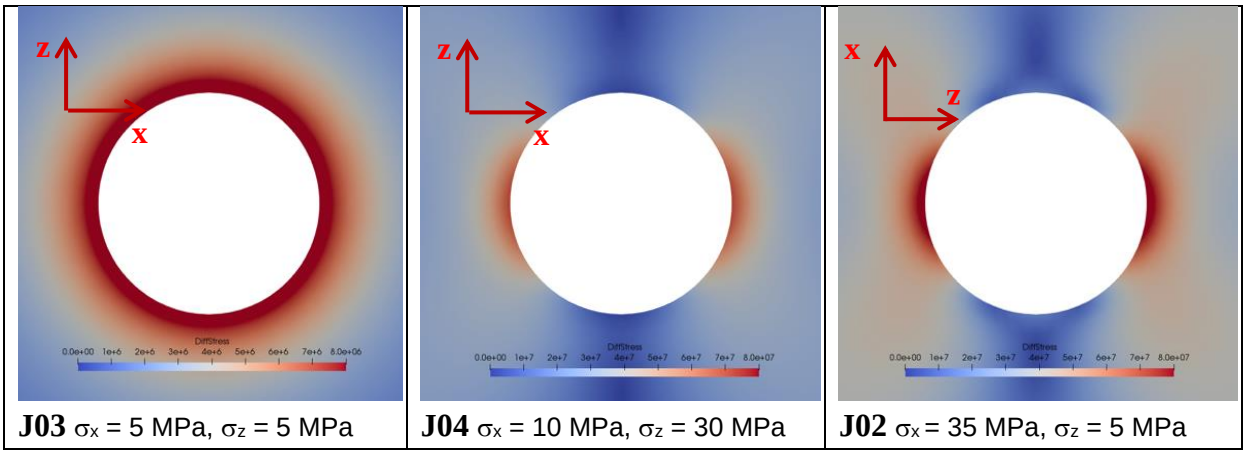

J03 σ_x = 5 MPa, σ_z = 5 MPa | **J04** σ_x = 10 MPa, σ_z = 30 MPa | **J02** σ_x = 35 MPa, σ_z = 5 MPa

Figure 12. Idealised circular hole with plane strain FEM stress solutions considering stress states for the three triaxial jetting tests shown in Fig.11. Results confirm Kirsch solutions. For J03, the differential stress scale is an order of magnitude lower where the tangential stress is uniformly 10 MPa (Table 3).

4.4.2 FEM analysis of stress for observed jet-hole geometries

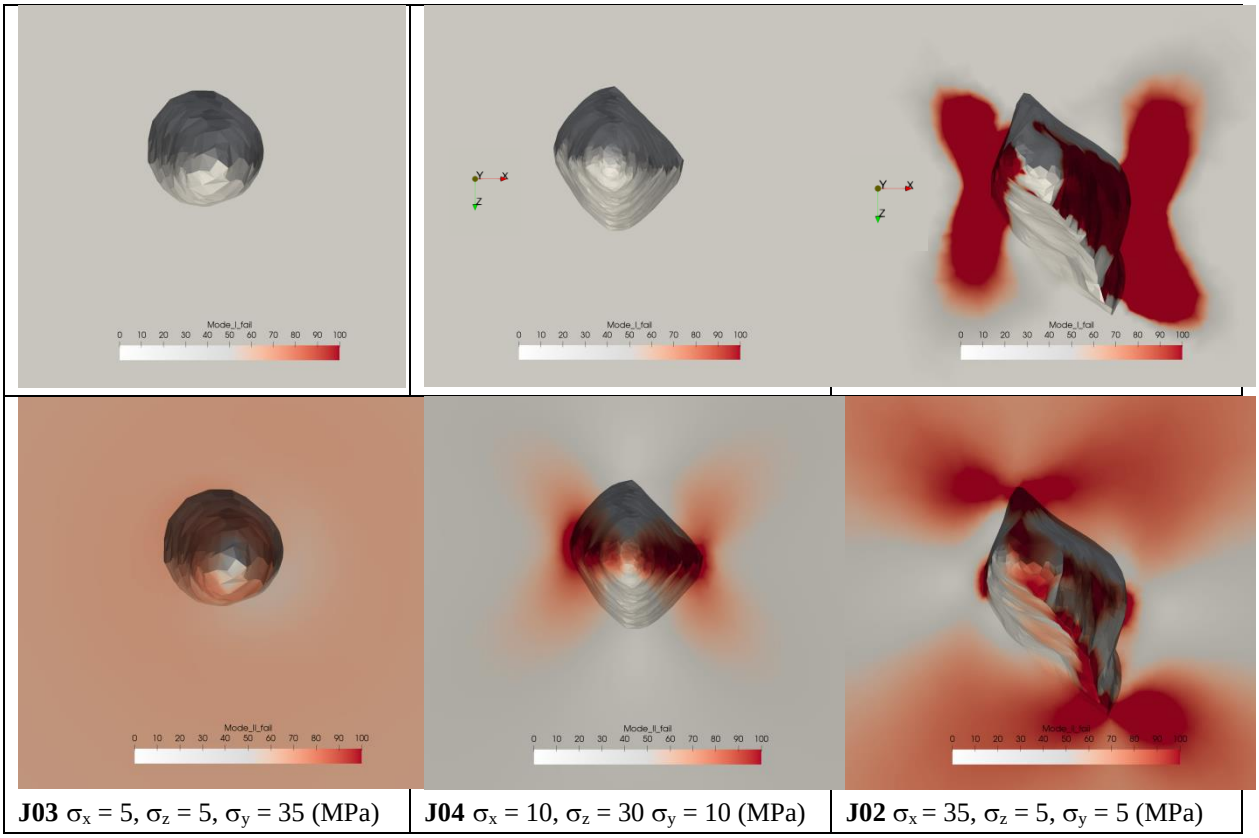

J03 σ_x = 5, σ_z = 5, σ_y = 35 (MPa) | **J04** σ_x = 10, σ_z = 30 σ_y = 10 (MPa) | **J02** σ_x = 35, σ_z = 5, σ_y = 5 (MPa)

Figure 13. FEM analysis of 3D stress field for observed jet-hole geometries. Stress magnitudes shown as cross section slice through jet-hole axis near end of hole. Also shown are stresses on internal wall surfaces as seen looking inside towards head of jet-hole. The three cases of triaxial in-situ boundary stresses used in experiments are presented. Stress level is shown normalized with respect to tensile strength as % of tensile stress required for tensile Mode I failure (top) and as % of the differential stress required for (Mohr circle with same mean stress to touch failure envelope for) initiation of shear Mode II failure (bottom) for Gildehaus Sandstone properties.

The SURE project has received funding from the European Union's Horizon 2020 research and innovation programme under grant agreement No 654662.

On examining the stress state around the actual jet-hole shapes generated prior to unloading the testing rig, the equilibrium states for these geometries and assuming the wall rock supports elastic deformations with no microstructural yielding, Fig. 13 (top right) suggests J02 would be under a state of significant incipient tensile cracking in the quadrants 90 degrees from the sharp breakouts due to a flexing of walls inwards towards the excavation. The geometry and stress levels in J04 show no such tensile stress tendencies. More significant is the analysis of incipient Mode II shear failure. J04 (Fig.13 bottom middle) is indicating no tendency to fail in shear in the top and bottom quadrants but is in a critical state for further incipient shearing and breakout deepening and widening, for example if boundary stress in the z-direction were to have increased slightly above 30 MPa. J02 (Fig. 13 bottom right) suggests the extreme sharp ellipse section shape is certainly under a critical state for further shear damage when the rig was unloaded, as would be expected. Looking at the surface of the hole from the inside, critical or near critical shear stress is seen in the acute angle seams of the breakouts in the top and bottom quadrants and at the head of the hole, suggesting the high insitu-stress ratio may be assisting the shearing ahead of the water jet irrespective of the effect of water pressure which is neglected here. One final observation of these J02 results is that near critical shear stresses are seen on the walls in the left-right quadrants where tensile stresses are higher, suggesting extensional shear may be possible.

Looking down J04 and J02 in Fig. 10, there is quite a lot of variability in geometry. Nozzle vibration may be influencing the profiles in J04, seemingly helping to broaden the hole top and bottom while the breakout corner is apparent on the left. For the J02 case with an exceptionally high stress ratio of 7:1, the extreme breakout looks like the dog-ears may be transitioning into compaction bands although another likely explanation is that tip extension is enhanced by water jet flow erosive action. Very locally in the tips, the differential stress computed from FEM (Fig. 13) appears high enough to continue to fail this rock in compression by shear. An alternative explanation is that the rock wall geometry from the CT scans includes locally failed rock that is not supporting elastic stresses, whereas maintained elastic properties are assumed in the FEM model.

4.4.3 Effect of non-linear shear failure envelope for Gildehaus/Bentheim Sandstone

For a Mohr-Coulomb failure criterion (linear) the unconfined compressive strength σ_c, cohesion C_0, and angle of internal friction ϕ are interdependent, see Eq (8). The reported laboratory average values given in Table 4 (below) are not self-consistent as by substituting $\phi = 23^o$ and $C_0 = 17.6$ MPa, we obtain $\sigma_c = 80$ MPa, however the laboratory result reported $\sigma_c = 53$ MPa. This suggests that the triaxial shear failure envelope is substantially non-linear with the pairing of $\phi = 23^o$ and $C_0 = 17.6$ MPa being a poor representation of behaviour at low confinement conditions. Ma & Haimson (2016) working with very similar Bentheim sandstone report that UCS tested specimens fail on planes at 10 degrees to σ_1. This means that for UCS = 53 MPa, at zero confinement conditions in jet-hole walls, $\phi = 70^o$ and therefore $C_0 = 4.67$ MPa may be a more appropriate pairing to give $\sigma_c = 53$ MPa rather than the reported

The SURE project has received funding from the European Union's Horizon 2020 research and innovation programme under grant agreement No 654662.

best fit linear envelope values of $\phi = 23^o$ and $C_0 = 17.6$ MPa (associated with $\sigma_c = 80$ MPa) which is maybe more representative for shear failure of this sandstone at much higher confinements. In the simulations to follow using FDEM, a compromise pairing of $\phi = 30^o$ and $C_0 = 15.3$ MPa was adopted.

(In future work a nonlinear failure envelope criterion will be implemented in meso-scale homogeneous materials and behaviour more representative of Bentheim sandstone will be modelled. Development of microstructural modelling of inter-grain behaviour and pores in FDEM is considered under WP7.1)

4.5 FDEM modelling results

4.5.1 FDEM analysis – mesh and material properties

The FDEM simulation in this work is performed using a 2D plane strain analysis. Following a calibration process using uniaxial compression of rectangular specimens of 40 by 20 mm and element mesh size of ~0.5 mm, material property coefficients adopted for FDEM modelling were as given in Table 4.

The computational mesh used for the FDEM simulations was generated with the free software Gmsh. The 300x300 mm domain with the 20 mm borehole was defined using Boolean subtraction of a 20 mm disc from the 300 mm edge square. The Gmsh software allows the size of the mesh elements for each curve making a boundary to the computational domain to be defined. The mesh size was set to 20 mm on the boundaries of the domain, where a coarse mesh was sufficient to simulate the in-situ stresses. A mesh size of 0.5 mm was set on the boundaries of the borehole, up to a distance of 30 mm from the centre of the hole (Fig. 14)

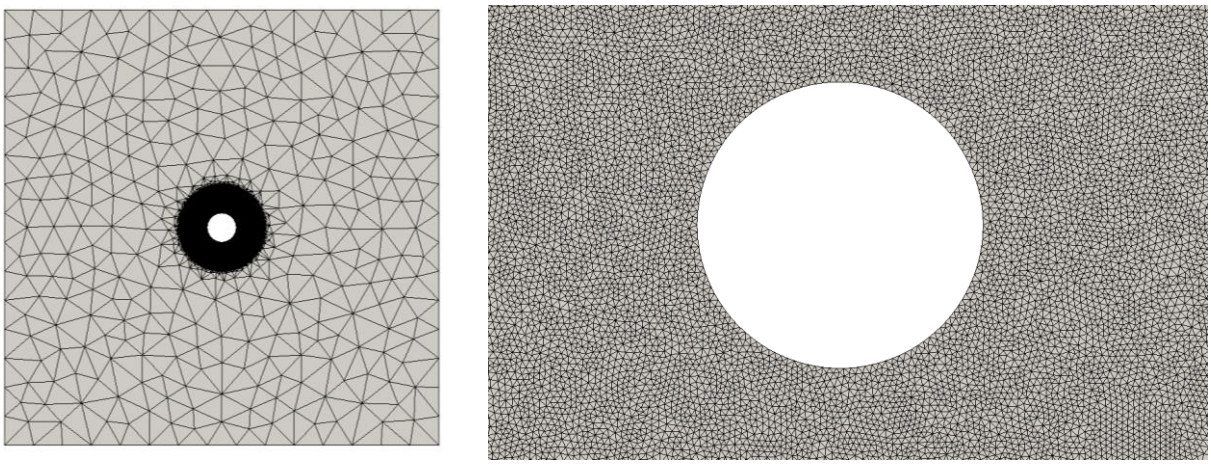

Figure 14. Mesh details of 300x300 mm block prepared using Gmsh. Right: enlarged view showing unstructured mesh refined to 0.5 mm elements up to 30 mm from centre of the 20 mm diameter hole.

The SURE project has received funding from the European Union's Horizon 2020 research and innovation programme under grant agreement No 654662.

Note that in Table 4, when modelling the jet-hole breakouts, the second (higher) set of GIc and GIIc values shown in brackets was used. These parameters represent the energy absorbed when a crack propagates. The increased values were substituted once brittle deformation has initiated. This can be justified as a means to help introduce more realistic energy absorption into the simulation that cannot be easily captured by FDEM because of probable sub-mesh scale microcracking occurring in the real sandstone specimens. Without such an increase, the simulation tends to portray very dynamic crack propagation and branching.

Table 4. Material properties of Gildehaus Sandstone obtained from Laboratory tests and values applied for FDEM simulation

Material Property	**Gildehaus Sst Lab**	**Gildehaus Sst FDEM**
Young's modulus E GPa	19.5	19.5
Poisson's ratio v	0.265	0.265
Bulk Density (kg/m^3)	2000	2000
Tensile strength MPa	3.5	3.5
Internal friction angle degrees	23	30
Cohesion MPa	17.6	15.3
UCS MPa	53	53
GIc J/m^2	8.2	15, (82)
GIIc J/m^2	171.7	171.7, (1717)

4.5.2 Stable breakout FDEM results for stress ratio 0.33 (or 3:1)

First, it is necessary to explain that the simulations are not without some background oscillations in stress levels. In Fig. 15, the block is shown after cracks have stabilised and when the applied stress magnitude at the boundaries is near to 33:11 MPa, whereas no breakouts had developed at 30:10 MPa. The stress ramping graph for a sample point (pink dot) half way between the bottom left corner and hole are shown in Fig 13b (bottom) indicating some oscillations in stress are remaining. These reduce in velocity and amplitude nearer to the hole, see Fig. 16. The period of these velocity oscillations is around 0.000025 s, which therefore generates a displacement amplitude of 0.005 mm. Although these small displacements should not have any significant effects on the simulation results, there still remains some doubt whether these much smaller oscillations have a negligible effect on the fracture process at the hole wall and a sensitivity analysis will be undertaken in the future.

The SURE project has received funding from the European Union's Horizon 2020 research and innovation programme under grant agreement No 654662.

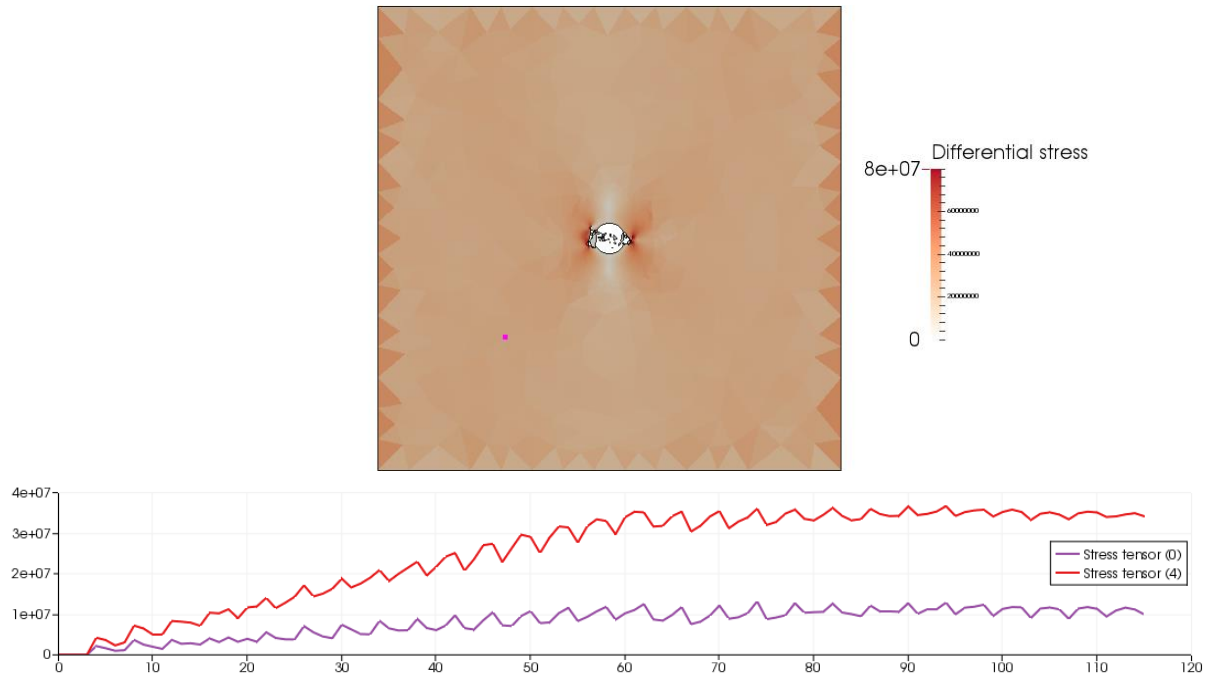

Figure 15. Block with fracturing stabilised after 115 steps (time increments), breakout fracturing beginning after 65 steps. Each step represents 0.000025 s so 100 steps equals 2.5 ms, Stresses are shown in Pa.

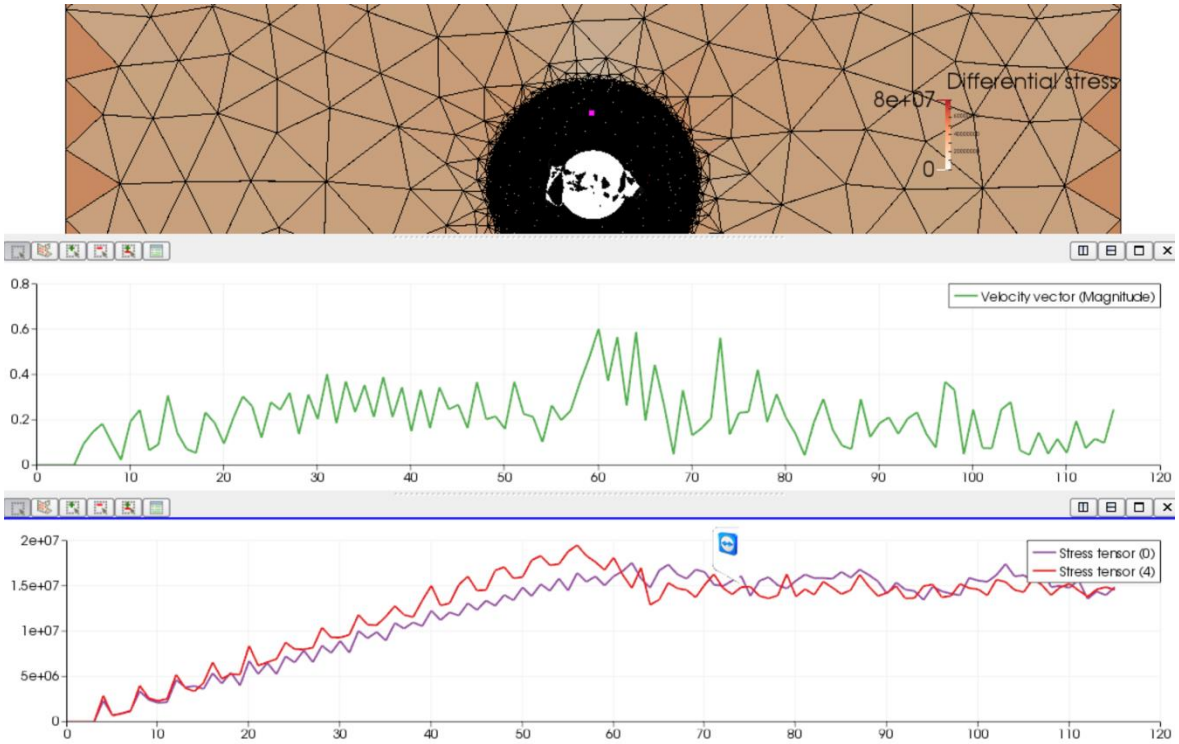

Figure 16. Closer view of block showing pink sampling point ~10 mm into wall with fracturing stabilised after 115 steps (time increments), breakout fracturing beginning after 65 steps after which no further increment is ramped up. Velocity in m/s and stresses in Pa, in x and z directions are shown for this sample point.

The SURE project has received funding from the European Union's Horizon 2020 research and innovation programme under grant agreement No 654662.

(Note that for J03, with a stress ratio of 1 (5 MPa, 5 MPa), the maximum stress values of about 10 MPa in the FDEM model bear out the FEM predictions of Fig. 11 and Fig. 12 where a uniform 10 MPa hoop stress is generated and therefore this FDEM result is of little interest and is not shown.)

The FDEM simulation results for progressive fracturing to create the breakouts for the 0.33 stress ratio are shown in Fig. 17. The simulation shows progressive fracture developments that are markedly not symmetric. Part of the explanation is the unstructured mesh that has initially optimally oriented mesh and joint elements for easy shearing in different locations on each side. The first breakouts occur when boundary stresses are at 33 and 11 MPa, the first fracture on each side initiating in shear. Invariably before milliseconds have elapsed, the propagating shear fracture initiates a wing crack at its tip, pointing back towards the hole. However, this does not absorb much of the stored elastic energy. The energy freed from unloading a loose fragment is negligible and a series of shear fractures in conjugate directions continues to deepen the breakout. Note that the fractures often marking the extremity of the breakout's width at each stage tend to be tensile cracks, which is an interesting observation possibly at odds with conventional understanding of breakouts. Finally, Fig. 17 (bottom) illustrates how the stress is refracted away from the weak hole and damaged rock and high differential stresses of ~70-80MPa are just supported in the abutting damaged but strong side regions before dropping to the expected uniform values of 20-30 MPa near the margins.

Fig. 18 shows how once the integrity of the elastic hoop stresses are broken down in the breakout region and at the expected maximum tangential hoop stress of ~80 MPa, a process of significant localised tensile stress build-up repeatedly develops near tips of new shear cracks. For each tensile area (deep blue) shown in the top middle and bottom frames of Fig. 18, a new tensile crack appears and tends to propagate towards the hole. Note that in the final frame of Fig. 17 we see this creating a large fragment and a very angular final profile on the left with a more typical 'dog ear' breakout on the right.

The final form of the stable enlarged breakout for this model with ~33:11 MPa when compared with the experimental jet-hole of J04 (Fig. 10) is not dissimilar and given that the water jet back-thrusters and comminuted sandstone fragments may have abraded the hole's walls considerably. The right angle breakout (right hand side) of the simulation is compatible with the laboratory test jet holes seen in J04 with almost right-angle corners if we assume the nozzle vibration has contributed to a more rounded enlargement in the z direction. The simulation results are broadly encouraging in terms of style and depth of breakout seen. They also raise the possibility that wing cracking is a major mechanism in enlarging breakouts.

The SURE project has received funding from the European Union's Horizon 2020 research and innovation programme under grant agreement No 654662.

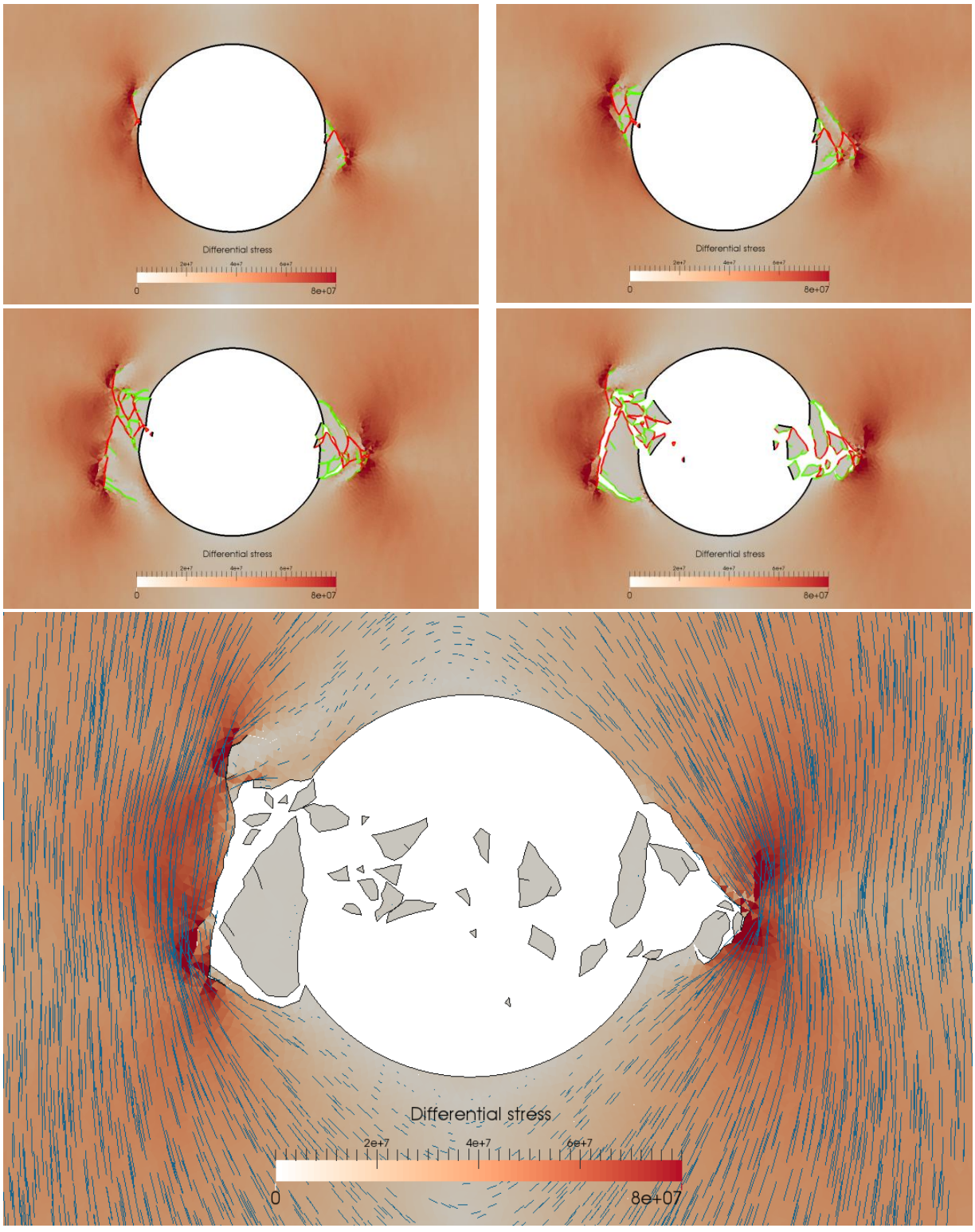

Figure 17. FDEM model of breakout for stress ratio 0.33 or 3. Sequence of progressive breakout and propagation starting at step 75 with far field stresses of about 33 and 11 MPa. Final frame (bottom) illustrated with sigma 1 stress trajectories after which no further stress ramping occurs and the fractures are stabilised. Red and Yellow lines indicate fractures initiating in shear and tension respectively.

The SURE project has received funding from the European Union's Horizon 2020 research and innovation programme under grant agreement No 654662.

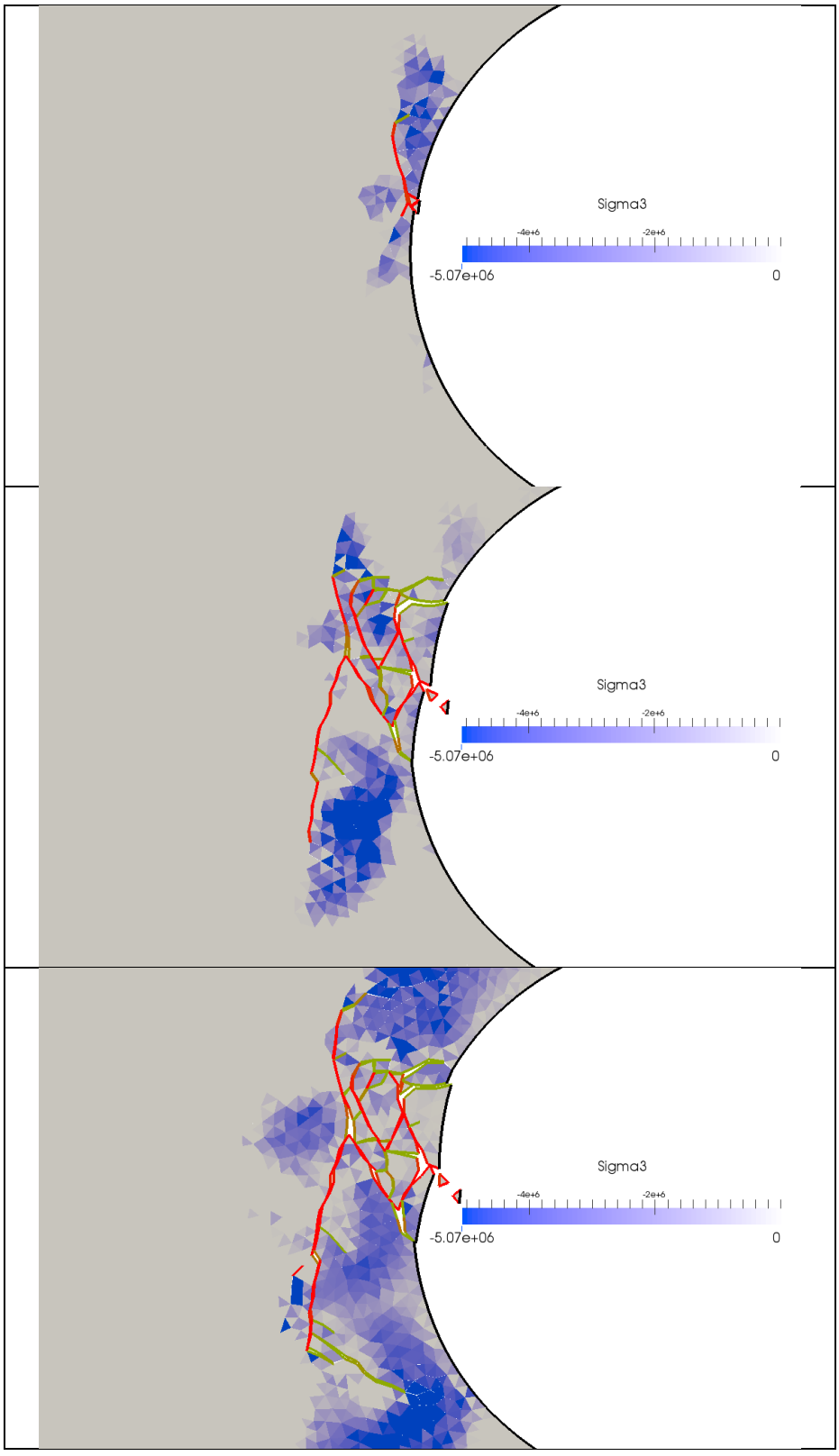

Figure 18. Progressive deformation with least principal stress showing tensile stress magnitudes (in blue colours). Fractures initiating in shear Mode II are shown in Red and in tensile opening Mode I in Yellow.

The SURE project has received funding from the European Union's Horizon 2020 research and innovation programme under grant agreement No 654662.

4.5.3 FDEM results for stress ratios 0.33, 0.14, 0.57 showing Unstable Collapse modes

The next series shows FDEM results where all three ratios have had the far field ramped to stress values slightly higher than those for breakouts and the simulation shows complete collapse behaviour in each case (Fig. 19). Unfortunately, in all three cases fractures propagate into the region of coarser elements and the simulations are not therefore as reliable. Consider first the 0.33 case we associate with J04. The top wall appears to stay quite well intact but the hole appears likely to fill with highly fragmented material of all sizes. Some resemblance to log-spiral shear fracturing is noted with some major fractures propagating towards the far field maximum applied stress.

For the 0.14 case associated with J02, the breakout pattern is remarkably similar to that seen in the experiments and the tensile cracks in the top and bottom wall are just as expected from the FEM analysis (Figs. 11 & 13). For J02, the stress ratio of 0.143, or 7 (35 MPa, 5 MPa) is a very extreme case designed to ensure breakout phenomena would be observed in the experiments. The ratio is well above that which is possible in terms of a tectonic setting for far field stresses. We anticipate from the Kirsch solution a well-developed tensile failure occurring in the x-direction $\sigma_{\theta^{min}}$ = -20 MPa (well in excess of Tensile strength (3.5 MPa) while breakouts by shear failure would be expected with $\sigma_{\theta^{max}}$ = 100 MPa. For this case, results shown in Fig. 19 appeared only partially capable of indicating the progressive development of the hole profile, results becoming numerically unstable prior to the full σ_x ramp of 35 MPa being achieved owing to the initial mesh refinement being inadequate at a certain distance from the hole. The breakout pattern started at σ_x = 30 MPa and develops sharp cusps as actually seen in J02 near the jet entrance to the block (Fig. 10). This is reminiscent of compaction bands. Furthermore, it is again possible that the jetted lateral's evolved shape from CT (scan cross-section, Fig. 10, right) may be influenced by the erosive forces of the water jet enlarging the excavated breakout features.

The simulation shows runaway cracking into the coarse mesh region. It is observed that while all the fragments are being driven into the hole, the hole itself appears stable as long as the large cracks do not continue to run. It seems unlikely that the experimentally jetted block with the 0.14 ratio (J02) developed any major cracks initiating from the tips of the breakouts and curving towards the major principal stress, but this could be interesting to check in future work as it is not totally clear with the longer penetrative fractures what is artefact and what is a plausible physical process. The overall impression is that FDEM illustrates a process of breakout shape development that could easily have occurred in the JO2 experiment and it would be worth investigating if tensile cracks observed in the simulation were visible in the microstructures of the jetted block. The major peripheral cracking that extends into the body of the rock block in the coarser meshed areas may well be an artefact of mismatched properties that impart overly brittle properties for this sandstone.

The SURE project has received funding from the European Union's Horizon 2020 research and innovation programme under grant agreement No 654662.

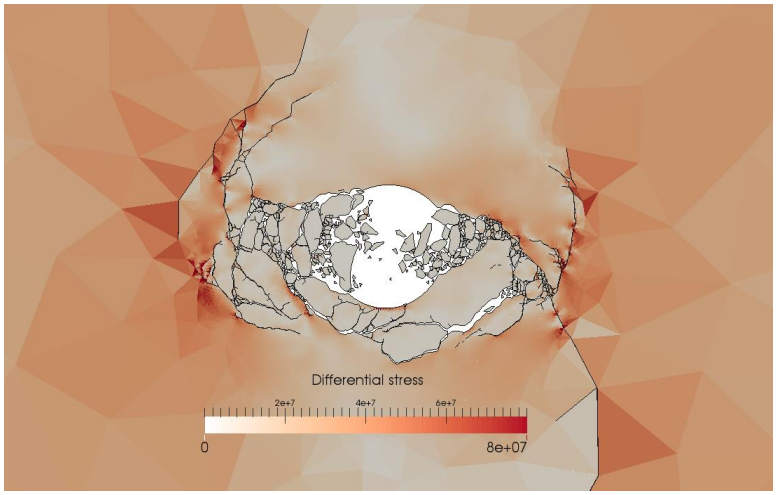

Stress Ratio 0.33, 3.0

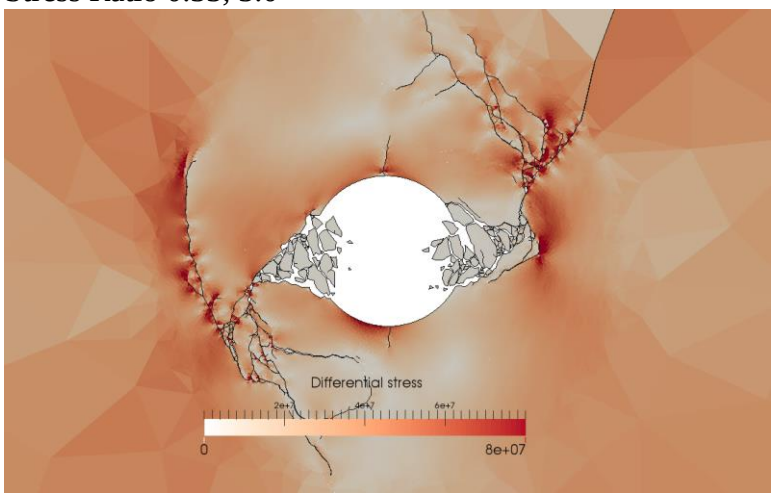

Stress Ratio 0.14, 7.0

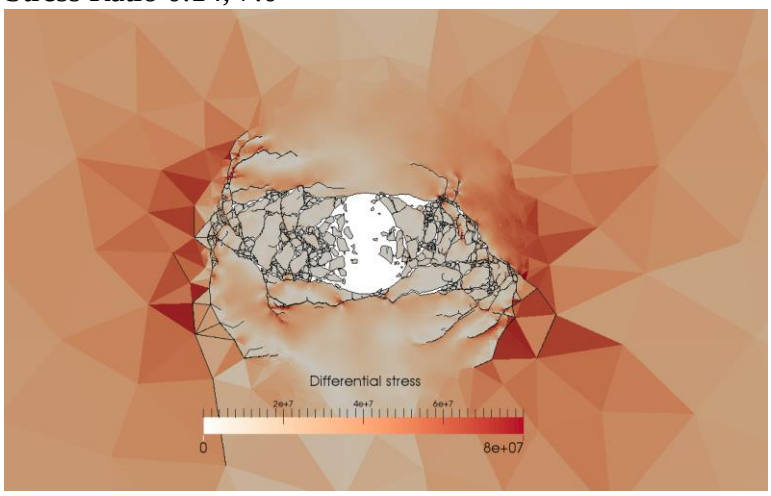

Stress Ratio 0.57, 1.75

Figure 19. FDEM results showing later stages of collapse behaviour for stress ramping at three different stress ratios.

The SURE project has received funding from the European Union's Horizon 2020 research and innovation programme under grant agreement No 654662.

In all three cases considered, for practical operations in the laboratory (and in the field) the jet nozzle and coil tubing may be expected to vibrate and create holes significantly larger than the nozzle diameter, as observed in J03 even under benign isotropic stress and low confinement i.e. easy drilling conditions. The right angle simulated breakouts of the J04 simulation are compatible with the laboratory test jet holes seen in J04 with almost right-angle corners if we assume the nozzle vibration has contributed to a more rounded enlargement in the z direction.

Finally the ratio 0.57 (1.75) was chosen as this represents the average stress ratio for the normal faulting regime. Again, the simulations show almost no reserve window of stability between beginning of breakouts and onset of collapse which occurs when the vertical stress is 36 MPa. The top wall rock is just intact but the progressive enlargement and deepening of the breakout sides has led to over half the hole being filled with fragments. Here it is possible to imagine the fragments reach a packing density in the hole that would start again to support some of the far field stress, a process which must happen in nature to limit the propagation of fracturing when a hole collapses.

4.5.4 Complex shape profiles

Preliminary simulations for a few complex shape sections were performed with the FDEM code subject to a ramping stress rising to 30:10 MPa. The simulation (Fig. 15) indicates a wall rock bearing a maximum differential stress of about 50 MPa in the jetted hole excavated in rock with Gildehaus sandstone properties. This result indicates that all the fracturing and or hole enlarging mechanisms that would have occurred in the original jetting tests have been completed, such that the hole under service conditions would be mainly stable and possibly quasi-stable at two extreme locations (hot spots in Fig 15.), with no threat to the serviceability of the hole.

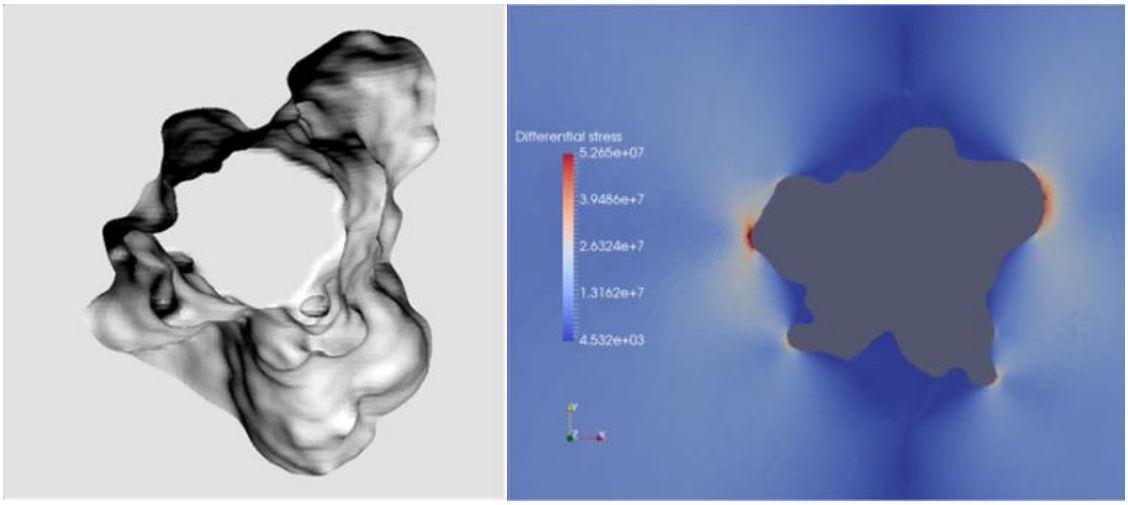

Figure 20. Visualisation from X-Ray CT and FEMDEM stress analysis of this profile showing no significant further fracturing is expected for a rock with UCS of about 55 MPa.

The SURE project has received funding from the European Union's Horizon 2020 research and innovation programme under grant agreement No 654662.

The fate of a star shaped hole of same area as a 20 mm hole in a 300 x 300 mm rock domain loaded in ramping to 30:10 is simulated for rock with Gildehaus properties (Fig. 21). The simulation shows that the large vulnerable segments between unfavorably positioned star arms are prone to being sheared off early compared to breakouts in circular holes and that the star shaped hole is likely to be rapidly enlarged. It is unclear how the breakage pattern would evolve as peripheral cracks extend into coarse mesh prematurely ending the simulation. It is suggested that in general, the more sharply cornered and irregular the hole's cross section left by jetting back-thruster action, the more likely there will be large fragments breaking off during a ramping up of stress levels possibly prior to stress levels needed for breakouts to begin in an equivalent more circular initial hole.

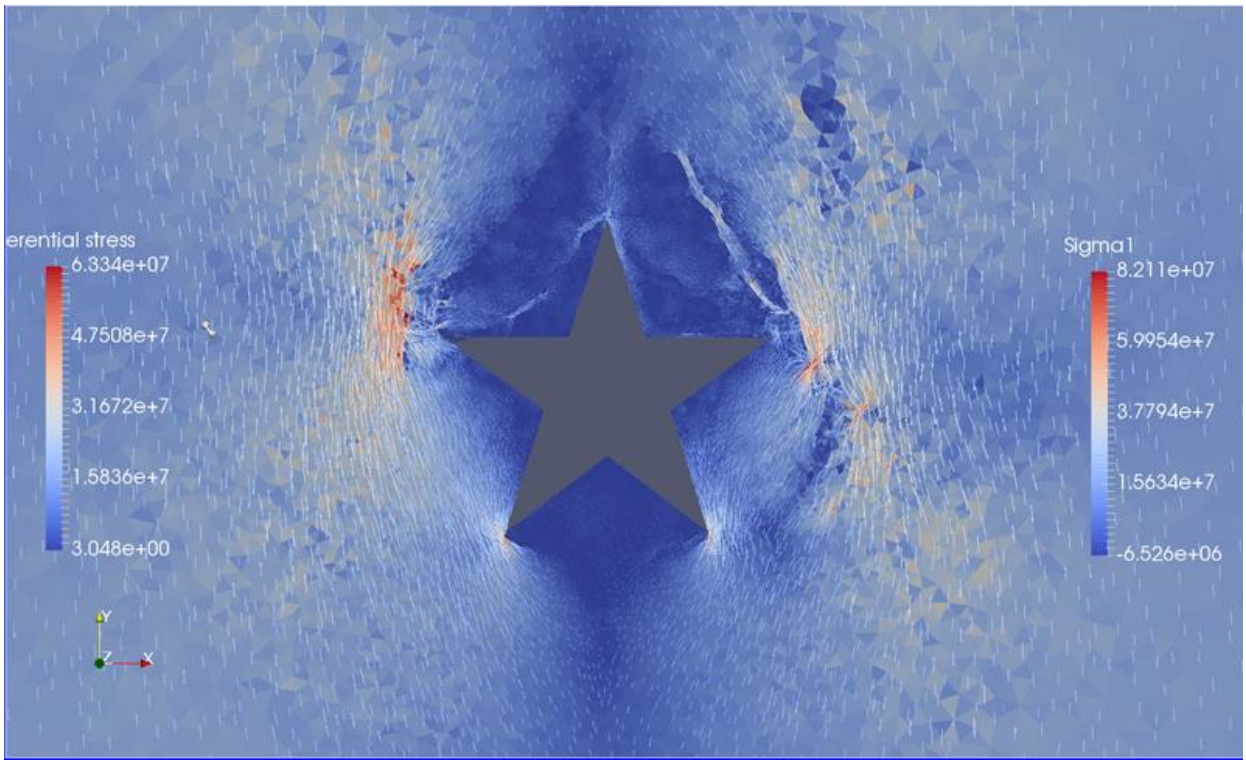

Figure 21. FDEM simulation of stressing of star-shaped hole with ramping at ratio 3:1 vertical to horizontal. Two major fragments developed between top left and top right arms. Sigma 1 stress trajectories refracted. Stress shadow in lower unstressed region.

4.6 Discussion

The ability of the FDEM simulation to illustrate the details of sequential crack interactions and breakout development mechanisms is shown to be excellent. Especially interesting and a new observation was the tendency for initial shear fractures to develop and propagate and at their tips, encourage tensional wing cracks to isolate fragments that break away. A more conventional understanding, certainly for less brittle rocks, is that almost simultaneous progressive conjugate shears push out material leaving increasingly large wedge shaped breakouts.

The SURE project has received funding from the European Union's Horizon 2020 research and innovation programme under grant agreement No 654662.

A new coupled protocol tool (Section 4.2.4) for using FEM to speed up FDEM simulations has been tested. The tool was developed in the context of a requirement to stress an already holed rock domain under a ramping of boundary stresses from an unstressed state, at a given stress ratio and in a series of increments. The FDEM simulation results achieved to date with this protocol indicate that for this loading history, once fracturing begins, it tends to propagate and grow into a pattern reminiscent of breakouts, but that the breakouts tend to propagate persistent cracks unstably away from the hole. Even with small increments of ~2 MPa vertical and 0.67 MPa horizontal applied at the boundary of a 300 mm block, with only very small amplitude stress waves arriving at the hole (made small by virtue of the coupling protocol design), the FDEM simulation often generates increasingly extending cracks, once fracturing has started with no further boundary stress increments being necessary to drive them. This numerical behaviour is a surprising contrast to what we know from experiments; that the sandstone's unconfined compressive strength (53 MPa) and shear failure envelope properties and block size relative to the hole are sufficient for the stress levels of 30 and 10 MPa which only produced modest breakouts. The results are in this sense problematic and we have to question why the differences occur. Several key factors meaning the simulations are not properly set up to capture the real behaviour tested in the laboratory are now considered in addition to the obvious simplification of 2D analysis.

(i) Ramping up stress around a hole from zero is not the same as perturbing an equilibrium far field stress by material removal during jetting. The same considerations make phasing the loading history for modelling tunnel stability also difficult but procedures do exist in the literature for perturbing by unloading.

(ii) The transient dynamic capturing FDEM code responds to rapid boundary deformations applied over several milliseconds and models the resulting stress waves caused by any sudden crack propagation. The relatively slow rates of stress increase and take-up of wall stress during jet-excavation of holes is likely to be mainly a quasi-static deformation loading process that is modelled several orders of magnitude faster in FDEM but hopefully still within rates that lead to non-dynamic loading effects as a result of the new FEM/FDEM protocol. The material properties have been assumed to be rate independent.

(iii) The FEM/FDEM protocol, if using quite large steps, may be leaving behind an excessive amplitude of stress waves repeatedly feeding energy to the wall rock region even after the far field stress increments have stopped. Peak particle velocities for such vibrations are ~200 mm/sec but at incredibly high kHz frequencies near the hole wall the vibration displacements would seem almost negligible.

(iv) The behaviour of the weak porous sandstone in question is difficult to model as a meso-scale homogeneous brittle elastic material when no microstructure is included as the material

The SURE project has received funding from the European Union's Horizon 2020 research and innovation programme under grant agreement No 654662.

fracturing is more plastic than brittle. The model requires all the energy absorption by tensile and shear failure to occur on joint elements with energy absorbed during crack propagation controlled by GIc and GIIc and by friction sliding on new surfaces given by a friction coefficient of 0.6. Sub-element scale permanent deformation that absorbs energy is ignored such that in this work, to prevent catastrophic propagation the GIc and GIIc values for simulation need resetting above the UCS calibrated best values and well above laboratory specimen properties derived from fracture toughness tests.

(v) Ma & Haimson (2016) show this type of sandstone to have a highly non-linear shear failure envelope in triaxial tests and for uniaxial conditions, fractures formed at just 10^o to σ_1, suggesting an angle of internal friction of $\phi = 70^o$ (Section 4.4.3). But in this study, the computer code would not execute correctly with such a high value. It will certainly change the simulated behaviour near the unconfined wall-rock if this value of ϕ and the lower C_0 pairing can be used rather than the pairing for higher confining stresses. The FDEM code should be run with a non-linear Mohr-Coulomb type shear failure criterion but this has yet to be implemented.

FDEM simulations have produced results broadly in agreement with the WP4, WP5 triaxial test breakout features. Tests and simulations were performed under similar in-situ stress conditions with 30:10 MPa and 35:5 MPa, but the material properties assigned need further adjustment to benefit fully from the FDEM's ability to test the evolution of jet-hole wall damage and to better understand conditions leading to unsustainable and collapsing jet-holes.

The simulations produced a rapidly progressing failure response more typical of a stronger more brittle rock with much stored strain energy being released suddenly in a high stress regime. The FDEM simulation may be altogether much better at predicting brittle stronger jet-hole wall rock. To mirror experimental observations in porous sandstones, it would be expected that the simulations begin with small conjugate shear breakouts that would only progress to wide breakouts with stable hole enlargements over significant ramping up of the applied far-field stresses, but this was not observed. It remains for future work to investigate further if this is due to artefacts of the code or to incorrect assignment of physical properties for this weak poorly compacted sandstone and whether the ramping up simulated loading history is fundamentally unable to represent the take up of increasing differential stress in the walls of the jethole as they become established while the excavation passes through.

To check on the criteria from Section 3, for the Normal Faulting regime, a stress ratio of k_h = 0.57 was simulated with $\sigma_v > \sigma_{hmin}$. Simple theory with λ=0 predicts breakouts begin at 21.8 : 12.43 MPa, and collapse begins at 33.8 : 19.2 MPa for 53 MPa UCS rock i.e. at depths of 0.81 km, and 1.25 km. (or strictly, the equivalent but greater depth when λ=0.4 is substituted due to the pore pressure assisting stability by additionally confining the wall rock). The simulated response was that no breakouts occurred until σ_v= 36 MPa and then collapse swiftly

The SURE project has received funding from the European Union's Horizon 2020 research and innovation programme under grant agreement No 654662.

followed as the hole became completely unstable. This collapse stress is broadly in agreement with the simple theory prediction (33.8 MPa) which may be coincidental, and the onset of breakouts never materialised at 21.8 MPa for this less anisotropic stress case of 0.57. Further investigation into why breakout initiation was predicted well for ratios 0.14, 0.33 but not for 0.57 is needed.

The simple theory in Section 3 to predict depths for breakouts transitioning into wholesale collapse takes no account of the quite sudden stress redistributions that occur once the integrity of any approximately cylindrical wall-rock is compromised with significant unloading and stress relocation.

In future work, FDEM simulation research will focus more on investigating progression of breakouts through to a full wall collapse for different rock types. As shown in Section 4.5.3, FDEM has the capability of modelling the whole process and fragment debris filling of the excavated volume leading to an increased bulk density of fragments and eventual choking and stabilisation of the collapse process, as may occur in field operations. However, there is more to learn about how to get the most out of FDEM technology as a means of approximating highly complex physical process.

5 Conclusions

This research has raised the interesting possibility that an initially jetted hole may become enlarged through breakout instabilities. If the fragmentation by breakouts is occurring while sufficient energy from the jetting fluids is capable of comminuting and clearing the largest rock fragments, taking them away in suspended fluids in the return flow annulus, then to some extent breakout behaviour could be beneficial to enhancing heat exchange and higher rates of hot fluid flows. Simple theory suggests that greater than half the arch will be broken out if there is an excess of mean stress in relation to rock strength. This typically will occur when the sum of the principal stresses acting across the hole exceeds the UCS and sets an upper bound for field stress conditions (deepest viable jetting) for different in-situ scenarios i.e. rock strength, in-situ stress ratio, jetting direction. Simple equations and guide charts along the lines shown in this report can be devised to identify the bounds for breakouts and collapse states expected from a Kirsch equation theory and simplistic shear failure mode assumptions based on UCS.

Numerical simulation with elastic FEM is a useful aid to consideration of unusual hole geometries subject to predicted reservoir in-situ stress states as a simple elastic analysis can predict the percentage stress below critical stress for fracturing in the wall surrounds and leading jet-front faces of a borehole/jet-hole in 3D. A new non-commercial FEM tool was developed in MATLAB for this purpose and the ease of interpreting and visualising the results was illustrated. It was shown that the existing hole geometries with breakout features are in an equilibrium state that would suggest the breakouts deepen with the slightest increase in

The SURE project has received funding from the European Union's Horizon 2020 research and innovation programme under grant agreement No 654662.

background stresses, which must be true of all jet-holes that have some degree of breakout features.

A new coupled protocol tool for implicit FEM – explicit FDEM was developed and deployed for this research for FDEM modelling of progressive fracture and fragmentation. The advantage is that a large part of the elastic analysis that would be very slow to solve in explicit FDEM can be solved quickly with an implicit FEM solver, enabling the FDEM simulation with ramping of loads to be executed much faster than a pure FDEM simulation, with minimal unwanted dynamic effects associated with the boundary stress loading.

FDEM simulation highlights the simple theory's lack of consideration of progressive deformation and stress redistribution effects once fractures initiate, suggesting the second simple criterion given in Section 3 for collapse states may be too simplistic and the safe window between initiation of breakouts and collapse may be quite false. However, the possibility exists that FDEM simulation artificially hastens the onset of collapse because elastic energy is not sufficiently dissipated locally during breakout deepening.

FDEM results were especially interesting in showing a previously undocumented mode of progressive breakouts based on alternating shear fracturing with tensile wing crack loosening and the formation of discrete fragments that are seen to move into the hole.

FDEM simulation of borehole wall stability using Solidity has been examined with the properties of just the one rock type, the Bentheim sandstone (from Gildehaus Quarry) which is a weak (UCS = 53 MPa) poorly compacted friable highly porous (~20%) sandstone with a nonlinear failure envelope in confined triaxial stress states. This rock was selected because jet drilled holes in several true-triaxial stress states were available and breakout features were developed, yet the holes were clearly stable enough to function in geothermal reservoirs. The FDEM modelling suggests the experimental holes are closer to conditions for collapse instability than seems likely from the observed experimental holes and wallrock. There remain several factors that mean the FDEM modelling and the approach to introducing the wall stress state history into the computational domain leads to results that are inconclusive when applied to real jetted holes and these were discussed at length in Section 4.6. They include the use of loading history rather than unloading and the apparent inability of the simulation to absorb elastic energy realistically for the sandstone in question.

Further numerical simulation using FDEM tools informed by 3D stress fields in wall-rock behind a jetted front and more realistically phased loading histories are planned for future work. Such studies may help provide an understanding and better prediction of when the field stress to strength ratio conditions are simply too high for practical operations.

6 Acknowledgements

The SURE project has received funding from the European Union's Horizon 2020 research and innovation programme under grant agreement No 654662. The content of this report reflects only the authors' view. The use of X-Ray CT data from true triaxial jetting tests

The SURE project has received funding from the European Union's Horizon 2020 research and innovation programme under grant agreement No 654662.

DOI: 10.2312/GFZ.4.8.2019.009

undertaken by Simon Hahn (GZB) and Richard Bakker (TUDelft) for WP4 and WP5 is gratefully acknowledged.

7 References

Bakker, R R, Hahn S, Friebel M, Bruhn D. F., Reinsch, T & Barnhoorn, A. 2019. A laboratory study on radial water jet drilling in true triaxial stress conditions. *Geoscience Frontiers* (submitted)

Barton C. A. Zoback, M.D. Burns, K.L. 1988. In-situ stress orientation and magnitude at the Fenton geothermal site, New Mexico, determined from wellbore breakouts. *Geophysical Research Letters*, 15: No. 5, 467-470.

Baud, P. Reuschlé, T. Ji, Y. Cheung, C.S., Wong T.F. 2015. Mechanical compaction and strain localization in Bleurswiller sandstone. *J Geophys Res*, 120: 6501-6522.

Blöcher, G., Reinsch, T., Henninges, J., Milsch, H., Regenspurg, S., Kummerow, J. Francke, H., Kranz, S., Saadat, A., Zimmermann, G., Huenges, H. 2016. Hydraulic history and current state of the deep geothermal reservoir Groß Schönebeck, *Geothermics* Volume 63, 27-43.

Brehme, M., Regenspurg, S., Leary, P., Bulut, F., Milsch, H., Petrauskas, S., Valickas, R. & Blöcher, G. 2018. Injection-Triggered Occlusion of Flow Pathways in Geothermal Operations. *Geofluids*, Article ID 4694829, 14 pages.

Dresen, G., Stanchits, S., & Rybacki, E. 2010. Borehole breakout evolution through acoustic emission location analysis. *Int J Rock Mech Min Sci*, 47: 426–435.

Eberhard E. 2001. Numerical modelling of three-dimension stress rotation ahead of an advancing tunnel face. *Int J Rock Mech Min Sci*, 38: 499–518.

ELFEN, 2011. Rockfield Software Ltd. ELFEN User's Manual. Swansea (UK).

Guo, L., Xiang, J., Latham, J. -P., & Izzuddin, B. 2016. A numerical investigation of mesh sensitivity for a new three-dimensional fracture model within the combined finite-discrete element method. *Engineering Fracture Mechanics*, 151: 70-91.

Haimson, B.C. and Cornet, F.H. (2003), ISRM Suggested Methods for rock stress estimation—Part 3: hydraulic fracturing (HF) and/or hydraulic testing of pre-existing fractures (HTPF). *Int J Rock Mech Min Sci*, 40: 1011–1020

Kim, H., Xie, L., Min, K-B. Bae, S. and Stephansson, O. 2017. Integrated In Situ Stress Estimation by Hydraulic Fracturing, Borehole Observations and Numerical Analysis at the EXP-1 Borehole in Pohang, Korea *Rock Mech Rock Eng* 50: 3141.

Kirsch, C. 1898. Die Theorie der Elastizität und die Bedürfnisse der Festigkeitslehre. *Zeitschrift des Vereines Deutscher Ingenieure*, 42: 797{807}.

Latham, J. -P., Xiang, J., Belayneh, M., Nick, H. M., Tsang, C. -F., & Blunt, M. J. Modelling stress-dependent permeability in fractured rock including effects of propagating and bending fracture. *Int J Rock Mech Min Sci* 57, (2013). 100-112.

The SURE project has received funding from the European Union's Horizon 2020 research and innovation programme under grant agreement No 654662.

Lei, Q., Latham, J.-P., & Tsang, C. F. 2017a. The use of discrete fracture networks for modelling coupled geomechanical and hydrological behaviour of fractured rocks. *Computers and Geotechnics* 85: 151-176.

Lei, Q., Latham, J.-P., Xiang, J., & Tsang, C. F. 2017b. Role of natural fractures in damage evolution around tunnel excavation in fractured rocks. *Engineering Geology*. 231: 100-113.

Lisjak, A., Grasselli, G. 2014. A review of discrete modeling techniques for fracturing processes in discontinuous rock masses. *J Rock Mech Geotech Eng*; 6:301–14.

Ma, X., & Haimson, B. C. 2016. Failure characteristics of two porous sandstones subjected to true triaxial stresses, *J. Geophys. Res. Solid Earth*, 121: 6477–6498.

Martin, C.D., Kaiser, P.K. & McCreath, D.R. 1998. Hoek–Brown parameters for predicting the depth of brittle failure around tunnels. *Can. Geotech. J.* 36: 136-151.

Medetbekova, M. Salimzadeh, S. Christensen, H.F. Nick H.M. 2017. Stability analysis of radial jet drilling in chalk reservoirs, Proceedings of the 6th Biot Conference on Poromechanics, Paris, France pp. 9-13.

Munjiza, A. 2004. The combined finite-discrete element method. John Wiley and Sons.

Munjiza, A. Andrews K.R.F. 2000 Penalty function method for combined finite-discrete element systems comprising large number of separate bodies. *Int J Numer Meth Eng*, 49:1377-1396.

Peters, E., Geel, C.R., Nair, R. & Blöcher, G. 2019. Potential of wells stimulation using small-diameter laters in geothermal reservoirs. European Geothermal Congress, Dan Haag, The Netherlands, 11-14 June 2019.

Rummel, F., Möhring-Erdman, & G. Baumgärtner, J. 1986. Stress Constraints and Hydrofracturing Stress Data for the Continental Crust. *PAGEOPH*, Vol. 124, Nos. 4/5, 876-895.

Setiawan, N.B. & Zimmerman, R.W. 2018. Wellbore breakout prediction in transversely isotropic rocks using true-triaxial failure criteria. *Int J Rock Mech Min Sci*, 112: 313–322.

Shen, B. 2008. Borehole breakouts and in-situ stresses SHIRMS 2008, eds. Y. Potvin, J. Carter, A. Dyskin, R. Jeffrey. Australian Centre for Geomechanics, Perth.

Shen, B. and Barton N. R., 2018. Rock fracturing mechanisms around underground openings *Geomechanics and Engineering*, 16:1, 35-47.

Shen, B., Stephansson, O. and Rinne, M. 2014, Modelling Rock Fracturing Processes: A Fracture Mechanics Approach Using FRACOD, Springer, 173.

Stacey, T.R. 1981. A simple Extension Strain Criterion for Fracture of Brittle Rock. *Int. J. Rock Mech. Min. Sci. & Geomech. Abstracts* 18:469-474.

Taherynia, M.H. Aghda, S.M.F. & Fahimifar, A. 2016. In-Situ Stress State and Tectonic Regime in Different Depths of Earth Crust. *Geotech Geol Eng*. 34: 679–687.

The SURE project has received funding from the European Union's Horizon 2020 research and innovation programme under grant agreement No 654662.

Tatone, B.S.A., Grasselli, G. 2015. A calibration procedure for two-dimensional laboratory-scale hybrid finite–discrete element simulations. *Int J Rock Mech Min Sci*, 75: 56-72.

Xiang, J., Munjiza, A., Latham, J-P. 2009. Finite strain, finite rotation quadratic tetrahedral element for the combined finite–discrete element method. *International Journal for Numerical Methods in Engineering* 79 (8): 946-978.

Zang, A., Stephansson, O. 2009. Stress field of the Earth's crust. Springer Science + Business Media BV, Dordrecht.

Zang, A., Stephansson, O. Heidback, O. and Janouschkowetz, S. 2012. World Stress Map Database as a Resource for Rock Mechanics and Rock Engineering. *Geotech Geol Eng* 30:625–646.

Zoback, M.D. 2007. Reservoir Geomechanics. Cambridge University Press, New York.

Zoback, M.D., Moos, D., Mastin, L. and Anderson, R.N. 1985. Well Bore breakouts and in situ stress. *Journal of Geophysical Research: Solid Earth*. 90: 5523-5530

Zoback, M.D., Barton C.A., Brudy, M. Castillo, D.A., Finkbeiner, T., Grollimund, B.R., Moos, D.B., Peska, P. Ward, C.D. & Wiprut, D.J. 2003. Determination of stress orientation and magnitude in deep wells. *Int J Rock Mech Mining Sci.* 40:1049–1076.

The SURE project has received funding from the European Union's Horizon 2020 research and innovation programme under grant agreement No 654662.